Taylor & Francis
Taylor & Francis Group

Finite-element model calibration of a railway vehicle based on experimental modal parameters

D. Ribeiro[a]*, R. Calçada[b], R. Delgado[b], M. Brehm[c] and V. Zabel[d]

[a]*School of Engineering, Polytechnic of Porto, Rua Dr. Bernardino de Almeida 431, 4200-072 Porto,
Portugal;* [b]*Faculty of Engineering, University of Porto, Rua Dr. Roberto Frias, 4200-465 Porto,
Portugal;* [c]*BATir – Structural and Material Computational Mechanics, Université Libre de Bruxelles,
Avenue Franklin Roosevelt 50, 1000 Brussels, Belgium;* [d]*Institute of Structural Mechanics,
Bauhaus-University Weimar, Marienstraβe 15, 99423 Weimar, Germany*

This article describes the experimental calibration of a three-dimensional numerical model of an Alfa Pendular train vehicle based on modal parameters. The dynamic tests of the carbody and bogie of the vehicle allowed the determination of the frequencies and modal configurations of 13 vibration modes, by applying the data-driven stochastic subspace identification method. In addition, a dynamic characterisation test of the passenger-seat system was also conducted. The calibration of the model was performed using a submodelling/multistep approach involving two phases, the first one focused on the calibration of the model of the bogie under test conditions and the second one focused on the calibration of the complete model of the vehicle. The calibration was performed through an iterative method based on a genetic algorithm and allowed to obtain optimal values of 17 parameters of the numerical model. For the pairing of the vibration modes, real and complex, a recent technique was used based on the calculation of the modal strain energy. The stability of a significant number of parameters considering different initial populations demonstrated the robustness of the algorithm. The comparison of experimental and numerical responses before and after calibration revealed significant improvements in the numerical model and a very good correlation between the responses obtained with the calibrated model and the experimental responses.

Keywords: finite-element model updating; railway vehicle; dynamic tests; modal identification; mode pairing criteria; genetic algorithm

1. Introduction

When interacting with the railway track, moving trains induce vibrations that can affect the structural stability of the infrastructure and rolling stock components, the stability of the track and of the wheel–rail contact and passengers' comfort. Problems can occur on the plain track [1], on bridges [2–5] or on transition zones [6,7].

Dynamic models of the train-track coupled system are developed in order to perform an accurate analysis of the problems.

In this type of models the modelling of the vehicles is conducted based on formulations grounded on the multibody dynamics [8–10], on formulations based on the finite-element method [11–14] and also on hybrid formulations that combine both forms of modelling [15].

---

*Corresponding author. Email: drr@isep.ipp.pt

In formulations based on the multibody dynamics, the carbody, bogies and axles of the vehicles are modelled through rigid structures connected by springs and dampers which simulate the primary and secondary suspensions. Applications of such formulations can be found in the study developed by Wu *et al.* [16], on the modelling of conventional trains, and also Kwark *et al.* [8] and Lee and Kim [17], on the modelling of articulated trains.

In formulations based on the finite-element method it is possible to consider the deformability of the carbody, bogies and axles. Beam-finite elements arranged in a grid [18], as well as shell-finite elements [11,19,20] and volume-finite elements [11], have been used for modelling the carbody of the vehicle. The development of these models requires the knowledge of the geometrical and mechanical parameters of the vehicle's structure. This information, in most cases, is difficult to obtain from the vehicle manufacturers.

The use of models which consider the deformability of the carbody of the vehicle becomes more important due to the tendency to use increasingly lighter and slender structures in the manufacture of trains to reduce weight, construction costs, etc. [9]. Several authors such as Iwinicki [21], Carlbom [22], Diana *et al.* [23] and Tomioka *et al.* [18,20] showed that the flexural vibration of the carbody may contribute, in a large extent, to the accelerations that passengers are subjected to. The frequencies of these vibration modes range from 8.5 Hz to 13 Hz [12, 24–27], which is significantly relevant regarding human beings' sensitivity to vibration.

Diana *et al.* [23] showed that, due to the suspension of heavy equipment in the under-floor, there may be local vibration modes on the floor of the vehicle that can also affect passenger comfort.

Studies carried out by Carlbom [22] and Wei and Griffin [28,29] included the passenger-seat system in the models of vehicles. Carlbom [22] proposed several models for this system. In the simplest model, with one degree of freedom, the mass of the passenger is suspended by a spring and a damper. In the more complex model, with two degrees of freedom, part of the mass of the passenger is suspended by a spring and a damper while the other part (about 5–20% of the total mass) is not suspended. Wei and Griffin [29] conducted an extensive experimental study on the dynamic characteristics of the passenger-seat system that placed the range of the vibration frequencies between 3 Hz and 5 Hz.

The implementation of automatic procedures for the calibration of the numerical models of railway vehicles is still poorly reported in the bibliography. Iterative calibration methodologies based on optimisation techniques, such as the gradient-based techniques [11,30] or genetic algorithms [31], were used in the few identified studies.

The experimental identification of the modal parameters of the vehicles is usually performed considering the vehicle at rest or in motion. In tests where the vehicle is at rest excitation is induced by hydraulic actuators, electrodynamics exciters [11,19], impact hammers [11,14] or by the impact of other vehicles [32]. In tests with moving vehicles the excitation is induced by the irregularities of the track [32].

This article describes the calibration of a numerical model of an Alfa Pendular train vehicle base on modal parameters. The three-dimensional numerical model developed for the vehicle uses shell-finite elements for the carbody and beam-finite elements, together with spring-damper elements, in order to simulate the axles and bogies. This highly complex model also includes the modelling of the passenger-seat system.

The modal parameters of the vehicle were determined based on a set of forced vibration tests that focused specifically on the carbody, bogie and passenger-seat system. The calibration of the numerical model was conducted using a submodelling/multistep approach involving two phases: the first phase concerned the calibration of the model of the bogie and the second phase focused on the calibration of the complete model of the vehicle. The calibration methodology of numerical models involved a sensitivity analysis and an optimisation. The global sensitivity analysis was based on a stochastic sampling technique [33] and allowed the identification of the

numerical parameters that most affect the modal responses and, therefore, should be included in the optimisation of the model. The optimisation was carried out based on an iterative procedure using a genetic algorithm [34,35]. A mode pairing criterion based on the modal strain energy using the Enhanced Modal Assurance Criterion (EMAC) [36] was used to achieve the correct pairing of the numerical and experimental vibration modes. The implementation of this criterion, which was used in previous works of Brehm *et al.* [36] in structures with real vibration modes, was applied in this paper, for the first time, to structures with complex vibration modes based on a state formulation. The efficiency of this criterion, in comparison with classical Modal Assurance Criterion (MAC) [37], is demonstrated. Finally, the modal parameters of the calibrated numerical model are compared with the modal parameters of the initial numerical model.

2. The Alfa Pendular train

2.1. *General description*

The CPA 4000 series train, known as Alfa Pendular, exists since 1999 and connects Lisbon and Porto. Currently there are 10 units serving the public rail transport operator in Portugal (CP). This train consists of six vehicles, four motor vehicles (BAS, BBS, BBN and BAN) and two hauled vehicles (RNB and RNH). The train has a total length of 158.9 m and can reach a speed of 220 km/h. The total weight, in normal load conditions, is 323.3 t. The axle loads vary between 128.8 and 136.6 kN. Figure 1 shows a perspective of the Alfa Pendular train with the identification of all vehicles.

2.2. *BBN vehicle*

The BBN vehicle is a tourist class vehicle with a capacity of 62 passengers distributed into four alignments. Both bogies of this vehicle are motor bogies. The total mass of the vehicle, including the bogies, achieve 52.2 t, in running order, and 55.0 t, in normal load conditions. The length of the vehicle is 25.9 m. The distance between the bogie pivots of the vehicle equals 19.0 m and the wheelbase equals 2.7 m. Figure 2 shows a side view and a plan view of the BBN vehicle's interior.

The carbody is formed by a tubular structure made of aluminium alloy consisting of 20 alveolar extruded panels longitudinally welded. The seats are directly fixed to the carbody's structure through metallic joints. Figure 3 shows a cross-section of the structure of the carbody with the identification of its components: base (1), side walls (2) and cover (3), and further details of a joint between a side wall panel and a cover panel and also the details of a base panel.
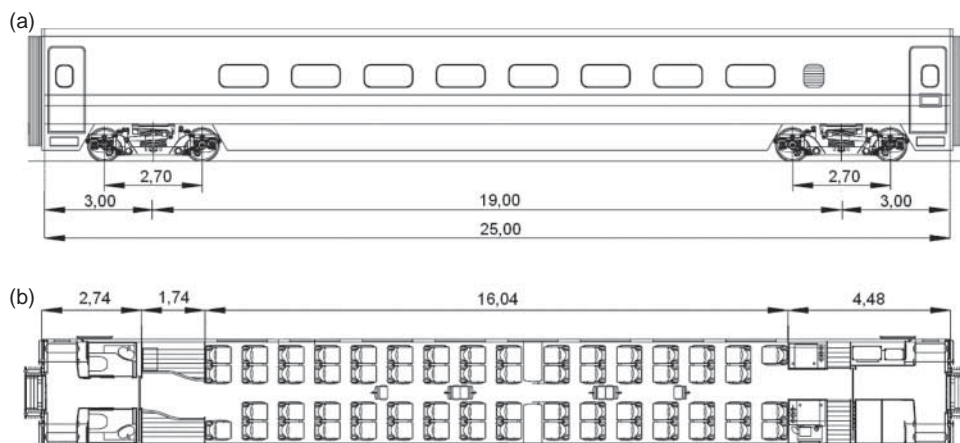

Figure 1. Alfa Pendular train.

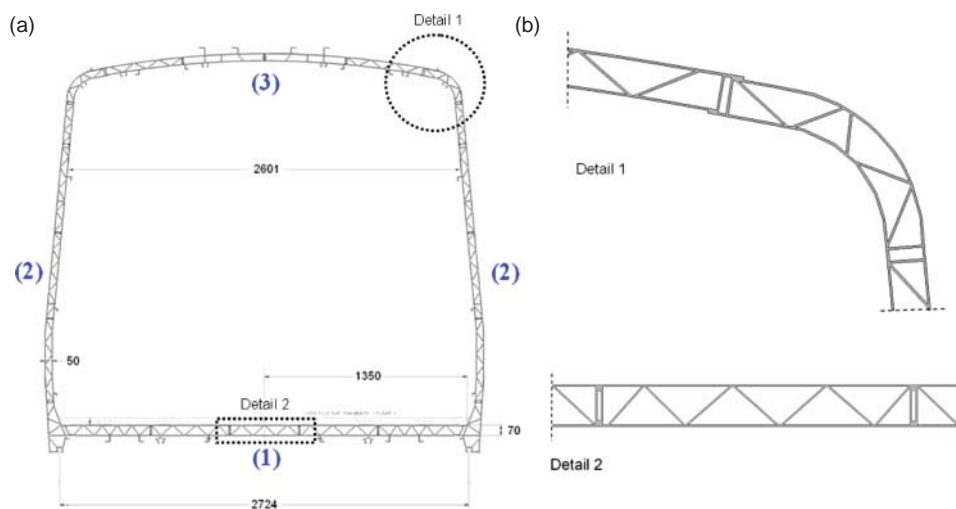Figure 2.   BBN vehicle: (a) side view; (b) plan view.

Figure 3.   Carbody: (a) cross-section; (b) structural details.

Figure 4 shows a schematic illustration of the bogie. The main structure, or chassis, is made of mild steel consisting of two girders (1) connected by two tubular crossbars (2), forming a double H structure. The connections between the girders' elements and between the girders and the crossbars are welded.

The bogie's chassis rests on two axles (3), specifically on the axle boxes (6) through springs (9) and dampers (10) of the primary suspensions and two traction rods, a lower one (7) and an upper one (8). In the axle box there is a bumpstop limiting the opening of the primary suspension springs.

Each bogie has two axles, one motor axle with a reduction gear unit (5) and two brake discs (4), and one trailer axle, with three brake discs. Figure 5 shows an image of a trailer axle. Joining the two girders there is a bolster which is articulated at the ends and also supports the calipers of the braking system.

The tilting bolster is supported over the chassis by secondary suspensions. The same tilting bolster, supports, in turn, the load bolster which is connected to the carbody of the vehicle.
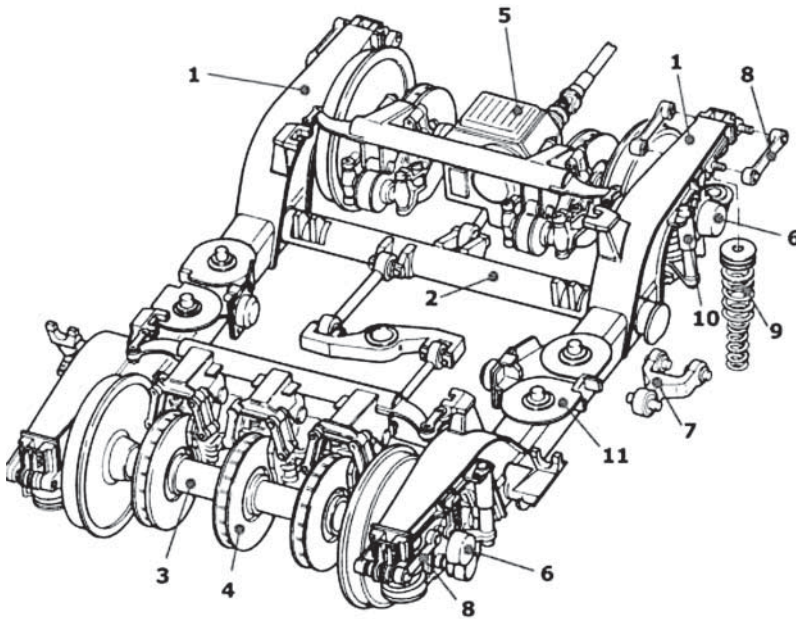
Figure 4.   Motor bogie [38].

Figure 5.   Trailer axle.

These two bolsters, linked by connecting rods and hydraulic actuators, allow the tilting of the carbody.

Figure 6(a) illustrates the connecting elements between the chassis and the tilting bolster (13), namely the springs (12) as well as a vertical (14) and a transverse (15) damper from the secondary suspension. The secondary suspension springs are supported by circular elastic blocks attached to the central area of the chassis (element (11) of Figure 4). The load bolster (17) rests on the tilting bolster through groups of connecting rods (18) which enable the rotation of the carbody around its longitudinal axis due to the action of two hydraulic actuators (19) (Figure 6(b)). The yaw motion of the carbody is prevented by two yaw dampers connecting the load bolsters to the girders. The carbody (16) is rigidly connected to the load bolster.

Table 1 shows the mass distribution in the BBN vehicle. The equipment located in the under-floor includes the engine and traction converter, the active suspension controller, the tilt and braking system controllers, the tanks and the air-conditioning system. The mass correspond-ing to coatings, bathroom equipment, electrical panels, cabinets, wiring, glazing, couplings,
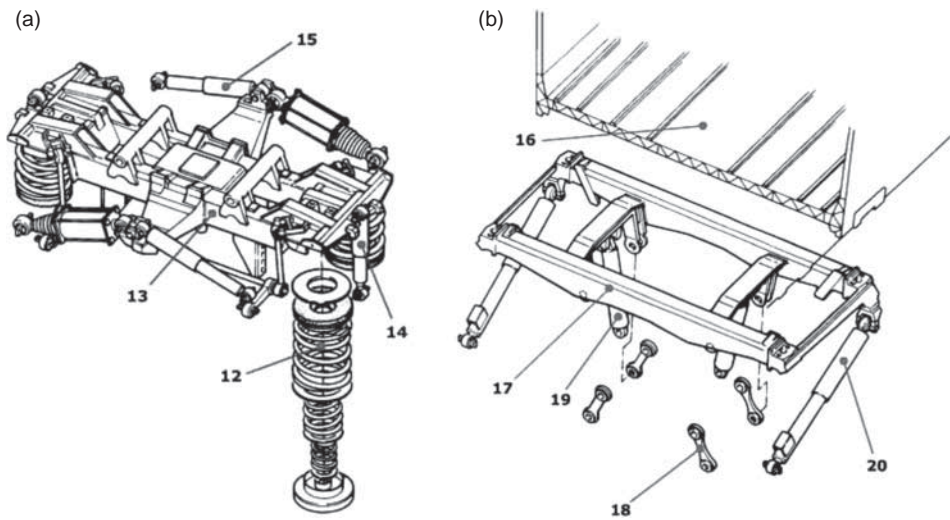
Figure 6.   Details of the bogie: (a) tilting bolster; (b) load bolster [38].

Table 1.   Mass distribution in the BBN vehicle.

Element	Component		Mass (kg)
Carbody	Structure (base, side walls and cover)[a]		6770
	Equipment	Seats[b]	1325
		Under-floor[a]	7851
		Others	19,694
Bogies[a]			16,560 (2 × 8280)
Axles and wheelsets[a]	Motor		1884
	Trailer		1538

[a]Estimated values based on the project's data.
[b]Values provided by EMEF.

protective covers, etc. was included in the item others under the component equipment. The mass of the bogies includes the masses of the axles and wheelsets.

3.   Numerical modelling

3.1.   *Description*

The modal analysis of the BBN vehicle was performed using a three-dimensional finite-element model developed in the ANSYS software [39]. The use of a finite-element formulation allows considering the influence of the deformability of the carbody, bogies and axles. Figure 7 presents a perspective, a side view and a top view of the numerical model.

The carbody was modelled by shell-finite elements while the bogies were modelled by beam-finite elements, with the exception of the suspensions, the connecting rods and the tilting system which were modelled by spring-damper assemblies. Additionally, the passenger-seat system was modelled, in a simplified manner, by a one-DOF system composed of a mass over a spring-damper assembly.

The masses of the equipment located in the under-floor of the carbody and bogies were simulated through mass elements. The structure was discretised with 1082 shell elements,
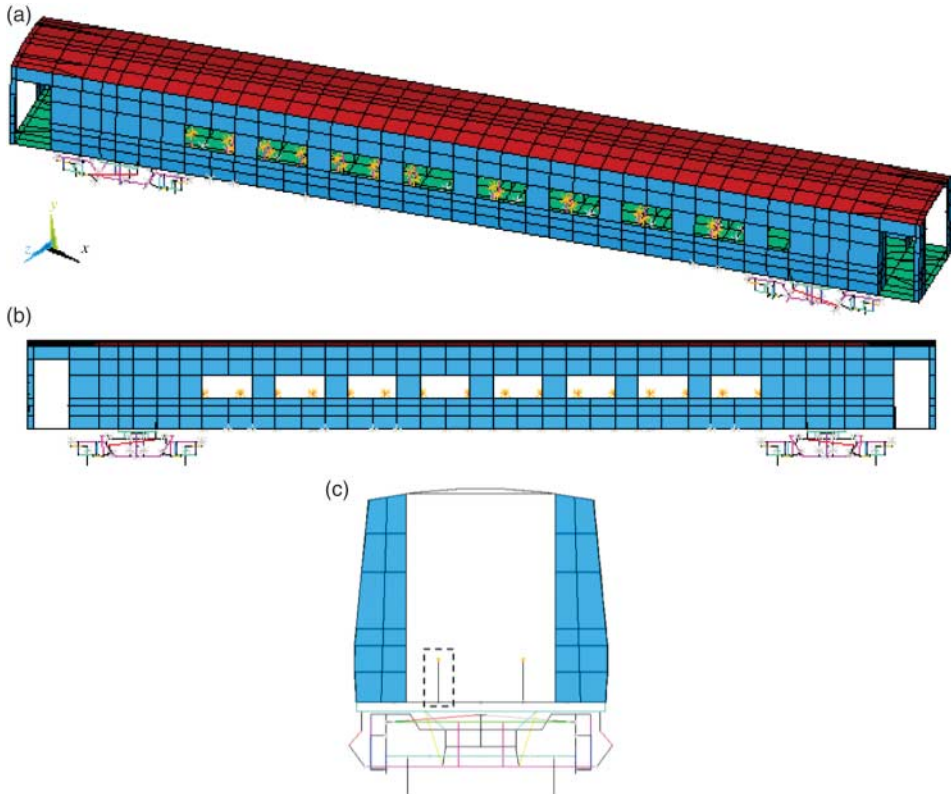
Figure 7.   Numerical model of the BBN vehicle: (a) perspective; (b) side view; (c) top view.

1029 beam elements and 148 spring-damper assemblies. The total number of nodes is 1902, corresponding to 10,704 degrees of freedom.

3.2.   *Carbody*

Table 2 presents the main geometric and mechanical parameters of the carbody's numerical modelling, including the designation, the selected value, the unit and the bibliographic references that were used. Additionally, the characteristics of the statistical distribution of some of the parameters, later used in the calibration phase of the model (see Section 6), are also shown.

Figure 8 identifies the panels of finite elements considered in the numerical modelling of the carbody in correspondence with the base, cover and side walls. In the modelling of the side walls special attention was given to the positioning of openings corresponding to windows and access doors.

The finite elements that simulate the various panels have length l and constant thickness e and are constituted by elastic and orthotropic materials. The thickness of each panel was determined based on the condition that the cross-sectional area of the finite-element panel is equal to the cross-sectional area of the real panel. The inertia correction of the panels, in directions x and z, was performed using the RMI parameter (Ratio of the bending Moment of

Table 2. Characterisation of the main parameters of the numerical model of the carbody.

| Parameter	Designation		Statistical distribution			Adopted value	Unit	Ref.
		Type	Average value/ standard deviation	Limits (lower/upper)				
K_{S1}	Stiffness of the vertical secondary suspension	Front bogie	Uniform	256.4/7.5	247/272.9	256.4	kN/m	[40]
K_{S2}		Rear bogie						
c_S	Vertical secondary suspension damping		Uniform	35/3.0	29.8/40.3	35	kN s/m	[40]
c_{AL}	Yaw suspension damping		Uniform	400/34.6	340/460	400	kN s/m	[40]
K_b	Stiffness of the tilting bolster-load bolster connection rod		Uniform	20,000/8660	5000/35,000	20,000	kN/m	[40]
ρ_{alum}	Aluminium density		–	–/–	–/–	2700	kg/m3	[41]
E	Modulus of deformability of aluminium		–	–/–	–/–	70	GPa	–
RMI_b	Corrective factor of the moment of inertia	Base	Uniform	225/101	50/400	90	–	[40]
RMI_p		Side walls	Uniform	90/34.6	30/150	114	–	
RMI_c		Cover	Uniform	300/57.7	200/400	386	–	
ΔM_b	Additional mass	Base	Uniform	70/11.5	50/90	70	%	[40]
ΔM_p		Side walls	Uniform	20/8.7	5/35	20	%	
ΔM_c		Cover	Uniform	7.5/4.3	0/15	10	%	
e_{bas}	Equivalent thickness	Base	–	–/–	–/–	10.2	mm	–
e_{par}		Side walls	–	–/–	–/–	10.3	mm	–
e_{cob}		Cover	–	–/–	–/–	8.8	mm	–
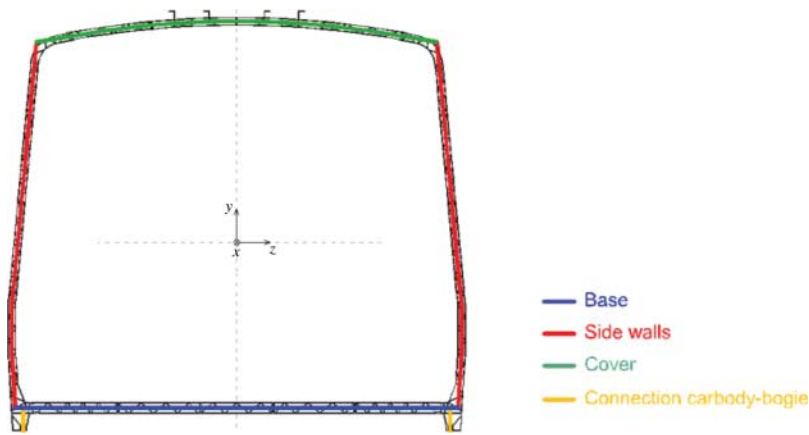
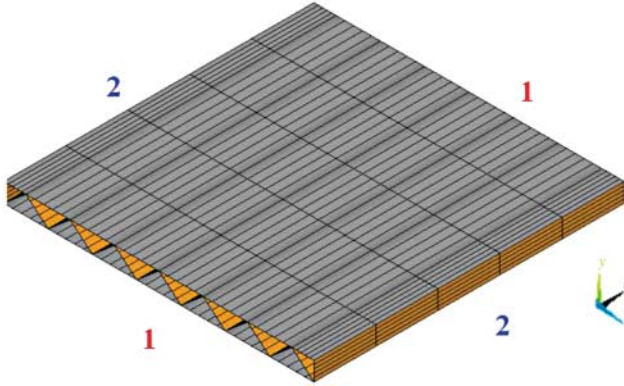Figure 8. Finite-elements panels from the numerical modelling of the carbody.

Figure 9. Numerical model of a portion of the carbody's panel.

Inertia) [39]:

$$\text{RMI} = \frac{I_{\text{real}}}{I_{\text{mod}}} \tag{1}$$

in which I_{real} is the real inertia of the panel and I_{mod} is the inertia calculated based on the thickness of the shell-finite element:

$$I_{\text{mod}} = \frac{le^3}{12}. \tag{2}$$

The finite-element model shown in Figure 9 was developed in order to evaluate the relation between longitudinal stiffness (direction x) and transverse stiffness (direction z) of the panels. The model refers to a portion of a base panel with a plan dimension equal to $1.0 \times 1.0\,\text{m}^2$. The lower, upper and diagonal plates were modelled using 3 mm thick shell-finite elements. The supports prevent translational movements in all directions and were positioned alternately on edges 1 and 2. Loading consists of a unit value vertical load, equally distributed, and applied to the upper plate.

The relation between the transverse and longitudinal stiffness was estimated based on the vertical displacement values of the central node of the panel, considering the supports placed on edges 1 and 2, alternately. The results revealed that the stiffness in the transverse direction is approximately 0.774 times the stiffness in the longitudinal direction. The same relation was applied to the side walls and cover panels.

The additional masses of the base, side walls and cover of the carbody refer to the mass parcels of the item others under the component equipment (Table 1) and were uniformly distributed on the surface of the respective structural elements.

The stiffness and damping parameters of the secondary suspension elements as well as their respective variation limits were estimated based on the values provided by the train's manufacturer [40].

3.3. *Bogie*

Figure 10 presents a perspective of the numerical model of the bogie. The chosen colours, combined with the legend, facilitate the identification of the different elements of the bogie.

The beam elements connecting the wheelsets to the axle box have zero stiffness around their axle, so as to simulate the linkage with the axle box. The support conditions imposed on
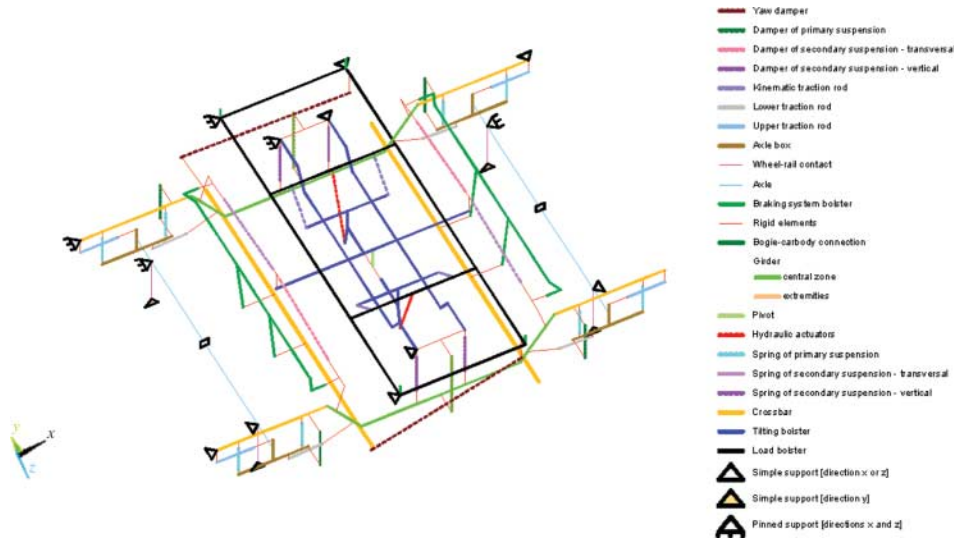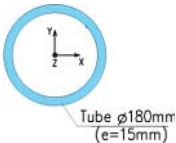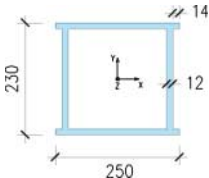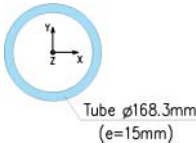
Figure 10.   Numerical model of the bogie.

Table 3.   Geometric characteristics of the structural elements of the bogies [40].

Element	Cross-section	Geometrical characteristics
Axle	Tube ⌀180mm (e=15mm)	$A = 0.00778\,\mathrm{m}^2$ $Ix = 0.267 \times 10^{-4}\,\mathrm{m}^4$ $Iy = 0.267 \times 10^{-4}\,\mathrm{m}^4$ $Iz = 0.534 \times 10^{-4}\,\mathrm{m}^4$
Girder (central zone)	14 / 12 / 230 / 250	$A = 0.01093\,\mathrm{m}^2$ $Ix = 0.857 \times 10^{-4}\,\mathrm{m}^4$ $Iy = 0.887 \times 10^{-4}\,\mathrm{m}^4$ $Iz = 0.121 \times 10^{-3}\,\mathrm{m}^4$
Crossbar	Tube ⌀168.3mm (e=15mm)	$A = 0.00718\,\mathrm{m}^2$ $Ix = 0.210 \times 10^{-4}\,\mathrm{m}^4$ $Iy = 0.210 \times 10^{-4}\,\mathrm{m}^4$ $Iz = 0.421 \times 10^{-4}\,\mathrm{m}^4$

the bogie, particularly on the girders and on the tilting and load bolsters, allow translational vertical movements and rotations around the *x* and *z* axes, preventing any other movements.

Table 3 shows the geometrical characteristics of the sections of the various elements that constitute the bogies, particularly the axles, girders and crossbars. The geometric characteristics are expressed in terms of the area (*A*) and inertias (*I*). The modulus of deformability and density of steel were considered equal to 200 GPa and 7850 kg/m^3, respectively.

Table 4 describes the main mechanical and geometrical parameters of the numerical model of the bogie, including designation, adopted value, unit and bibliographic references. Moreover,

Table 4. Characterisation of the main parameters of the numerical model of the bogie.

Parameter	Designation		Type	Average value/ standard deviation	Limits (lower/upper)	Adopted value	Unit	Ref.
				Statistical distribution				
K_P	Stiffness of the primary suspension		Uniform	564/26.6	518/610	564	kN/m	[40]
c_P	Damping of the primary suspension		Uniform	18/1.6	15.3/20.7	18	kN s/m	[40]
K_{bls}	Stiffness of the axle box connecting rods	Upper	Uniform	6.5/0.8	5.2/7.8	6.5	MN/m	[40]
K_{bli}		Lower	Uniform	25/2.9	20/30	25	MN/m	
K_{rc}	Stiffness of the wheel–rail connection		–	–/–	–/–	1.5674	$\times 10^9$ mN/m	[42]
ΔM_{lc}	Additional mass	Girder (central area)	Uniform	75/43.3	0/150	42	kg/m	[40]
ΔM_{le}		Girder (extremities)	Uniform	30/17.3	0/60	38	kg/m	
ΔM_t		Crossbar	Uniform	125/72.2	0/250	92	kg/m	
ΔM_e		Axles	–	–/–	–/–	271	kg/m	

the characteristics of the statistical distribution of certain parameters, which will be used in the model's calibration phase (see Section 6), are also indicated.

The stiffness and damping parameters of primary suspension elements and their respective variation limits were estimated based on information from the manufacturer [40]. The additional mass of the bogie, at the girders, crossbars and axles, is related to the mass of springs, dampers, connecting rods, links, reinforcement plates, axle boxes and others. These masses were linearly distributed in the different elements. In what concerns the girders the additional mass was further divided into two parcels according to their location: in the central zone, i.e. in the sections located between the crossbars and at the extremities.

The wheel–rail connection was modelled by a spring element with unidirectional behaviour.

3.4. *Modal parameters*

Table 5 shows the damped and undamped natural frequencies of the main vibration modes of the BBN vehicle. The damped frequencies are calculated based on a modal analysis that includes the damping matrix. In what concerns the bogies, for modes 1B and 2B, there are different frequency values according to the movement of the two bogies in phase and in antiphase, respectively. In the 3B mode, the different values of the frequencies are related to the isolated movements of the left and right bogies, respectively.

The modal results show differences between damped and undamped natural frequencies. These differences are more notorious for the rigid body modes of the carbody and bogies since these modes involve significant movements of the suspensions. In case of the bogies the differences are even more important since this additional damping is provided simultaneously by the primary and secondary suspensions.

Table 5.   Numerical natural frequencies of the carbody and bogies.

Element	Mode	Nature of vibration mode		Damped frequency (Hz)	Undamped frequency (Hz)
Carbody	1C	Rigid body	Rolling	0.86	0.82
	2C		Bouncing	1.04	1.00
	3C		Pitching	1.42	1.33
	4C	Structural	First distortion	10.21	10.21
	5C		First bending	16.20	16.20
	6C		First torsion	15.05	15.03
Bogies	1B	Rigid body	Bouncing	8.21/8.18	6.57/6.26
	2B		Rolling	4.89/5.28	4.09/4.53
	3B		Pitching	12.10/12.04	9.50/9.41
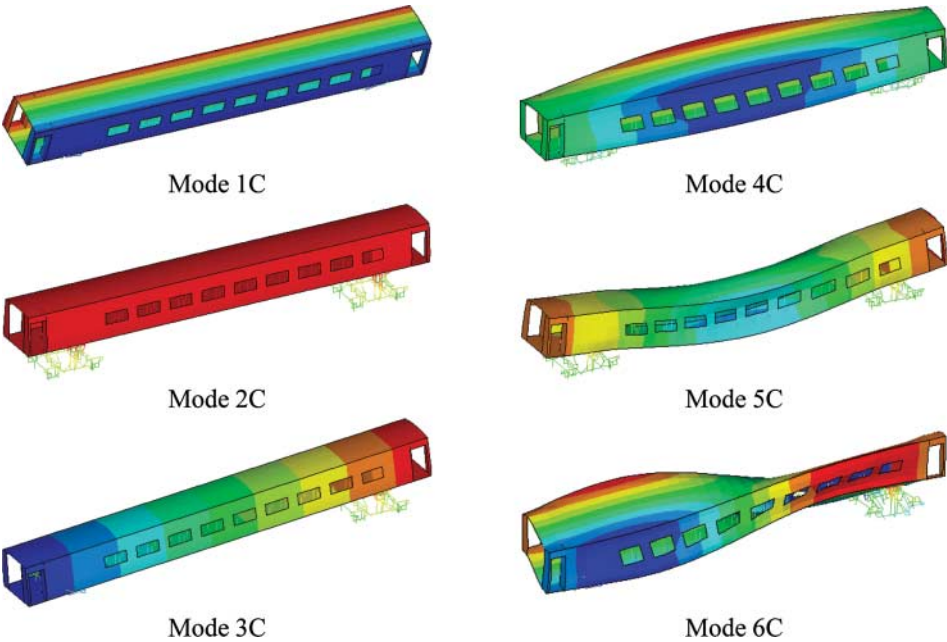
Figure 11.   Numerical rigid body and structural modes of vibration of the carbody.

Figure 11 illustrates the modal configurations associated with rigid body modes (1C, 2C and 3C) and structural modes of distortion (4C), bending (5C) and torsion (6C) of the carbody. In these modes the movements of the bogie have very low amplitude.

Figure 12 shows the modal configurations, in perspective and cross-section view, of a bogie of the vehicle. Mode 1B comprises the bouncing movement of the bogie. Modes 2B and 3B comprise the rolling and pitching movements of the bogie, respectively. In these modes the carbody shows very limited movements.

4.   Dynamic tests

This section describes the experimental tests of the BBN vehicle involving the dynamic tests of the carbody, bogie and passenger-seat system. The results of these tests will be used to calibrate the numerical model of the vehicle.
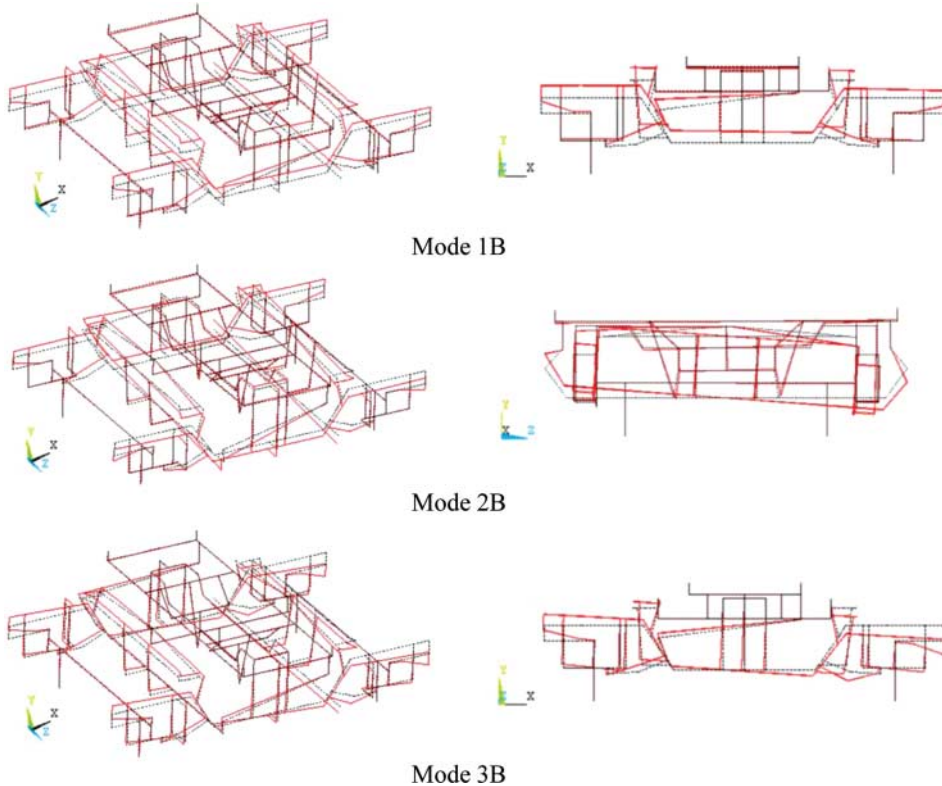
Figure 12. Numerical modes of vibration of the bogies.

4.1. *Carbody test*

The dynamic test of the carbody was conducted at EMEF facilities, in Porto, in order to identify the natural frequencies and vibration modes of the carbody involving rigid body and structural movements. EMEF is the company responsible for the maintenance of the CP trains. Figure 13 presents a perspective view of the tested vehicle. The mass of the carbody is equal to 35.64 t.

The carbody was instrumented with 14 PCB piezoelectric accelerometers (A0–A13), model 393A03, placed on the base of the carbody next to the intersection with the side walls, according to the scheme presented in Figure 14.

The accelerometers located within the area of the seats were positioned by means of metallic angles fixed to the structure of the seat with magnetic disks (Figure 15(a)). The accelerometers located at the ends of the carbody, in the access area, have been installed in steel blocks directly laid on the floor (Figure 15(b)).

The data acquisition was performed through the NI cDAQ-9172 system using three modules NI 9233 for IEPE type accelerometers. The time series were acquired for 12 min periods, with a sampling frequency of 2000 Hz, and then decimated to a frequency of 100 Hz.

Attending to the high damping of the vibration modes of the vehicle, it was necessary to use an external excitation in order to increase the vibration levels. That excitation was achieved through people jumping and, consequently, applying impulsive actions to the floor of the carbody.

Accelerometers were also installed on bogies, in this experiment, but due to accessibility restrictions it was not possible to excite the bogies with appropriate levels of vibration in order to facilitate the identification of modal parameters. It should be noted that the vibration modes

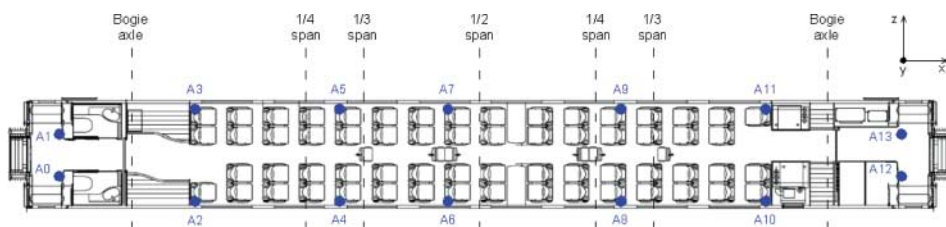Figure 13. View of the tested BBN vehicle.

Figure 14. Location of the accelerometers in the carbody of the vehicle.
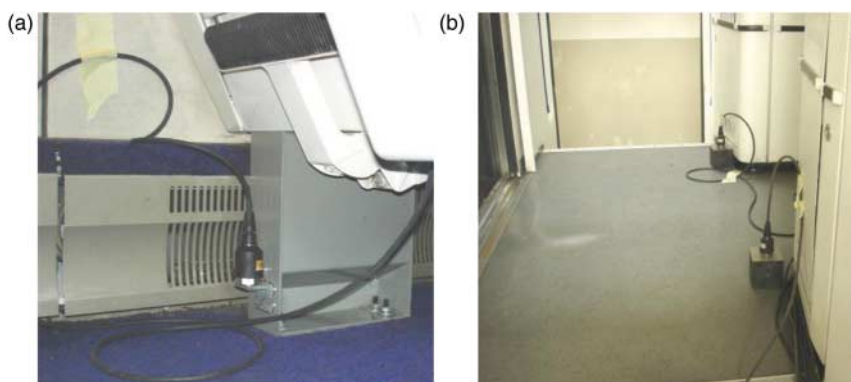

Figure 15. Accelerometers installed in the carbody of the vehicle: (a) seat; (b) floor.

of the bogies, within testing conditions, are considerably damped due to the dampers of both primary and secondary suspension systems.

The identification of the carbody's modal parameters was carried out through the application of the stochastic subspace identification method based on the time series of acceleration (SSI-DATA) available in the ARTeMIS software [43].

Figure 16 shows the stabilisation diagrams that were estimated based on state models of order between 1 and 160. The alignments highlighted in the figure correspond to the five vibration
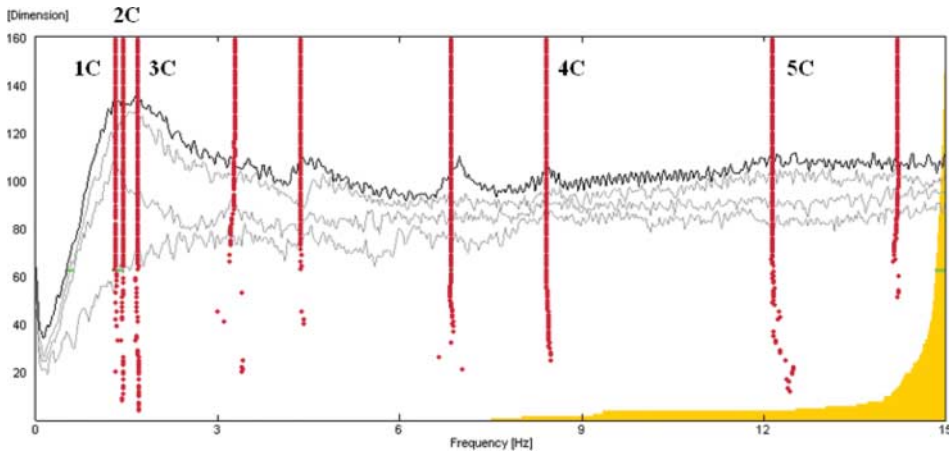
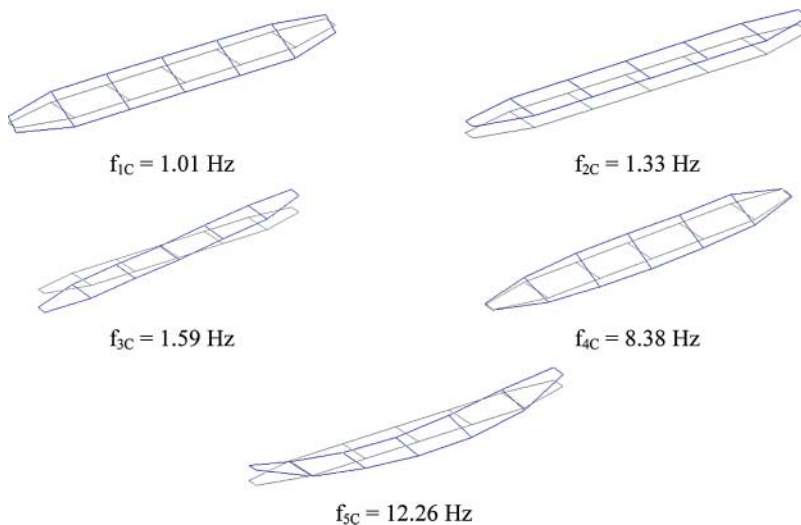Figure 16.   Identification of modal parameters through the SSI-DATA method.

Figure 17.   Experimental frequencies and vibration modes of the carbody.

modes of the carbody, which were identified due to this test, apart from other alignments associated with vibration modes of the seats and bogies.

Figure 17 illustrates the configurations of the identified vibration modes and the values of their natural frequencies. It was not possible to identify the mode of vibration 6C.

4.2.   *Bogie test*

The dynamic test of the bogie was performed in EMEF facilities in Entroncamento. Figure 18 shows an overview of the tested bogie and the reaction frame. Secondary suspensions, yaw dampers, tilting and load bolsters were disassembled in order to perform the test. Loads were applied to the bogie by two hydraulic actuators, in the area of the support blocks of the secondary suspensions, in order to reproduce the loads imposed by the carbody of the vehicle.
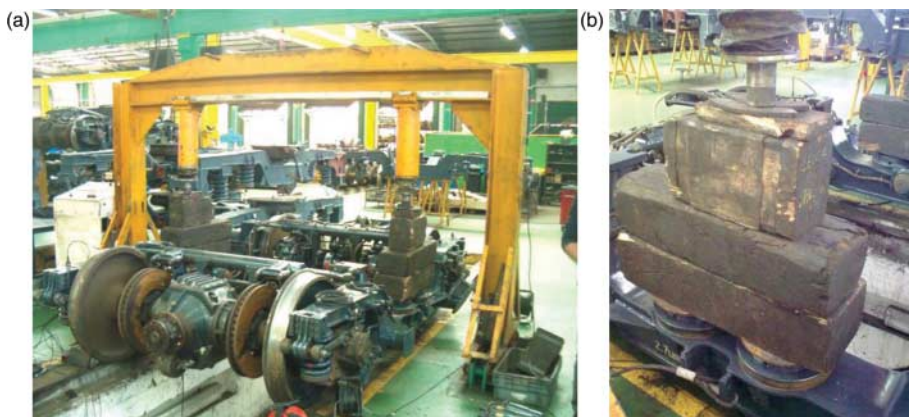
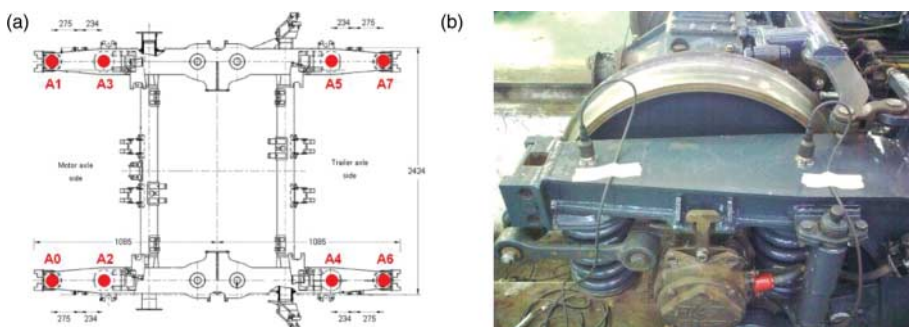Figure 18.   Dynamic test of the bogie: (a) overview; (b) actuator and distribution blocks.

Figure 19.   Dynamic test of the bogie: (a) plant with the location of the accelerometers; (b) detail of the installation.

This was also necessary to prevent the primary suspensions from being blocked by the axle boxes bumpstops. Each actuator applied a load equal to approximately 70 kN, which was constant during the test. The transfer of loads to the bogie was accomplished with the help of wood distribution blocks, as illustrated in Figure 18(b).

The test was conducted using eight PCB piezoelectric accelerometers (A0–A7), model 393A03, vertically positioned at the ends of the girders, as illustrated in Figure 19(a). Magnetic bases connect the accelerometers to the girders, as illustrated in detail in Figure 19(b).

The data acquisition was performed using the cDAQ NI-9172 system using two modules NI 9233 for IEPE type accelerometers, powered by a battery system. The time series were obtained through 5 min periods with a sampling frequency of 2000 Hz, and then decimated to a frequency of 200 Hz.

In order to excite the bogie, impulses were applied on its structure through rubber-tip hammers. Controlling the intensity of the impulses was essential to avoid saturation of the signals.

The test of the bogie was initially carried out with the primary dampers installed and, afterwards, without the dampers. The identification of the bogie's modal parameters, under test conditions, was also performed through the SSI-DATA method available in the ARTeMIS software.

Figure 20 shows the estimated stabilisation diagrams based on state models of order between 1 and 140, when testing the bogies without dampers (Figure 20(a)) and with dampers
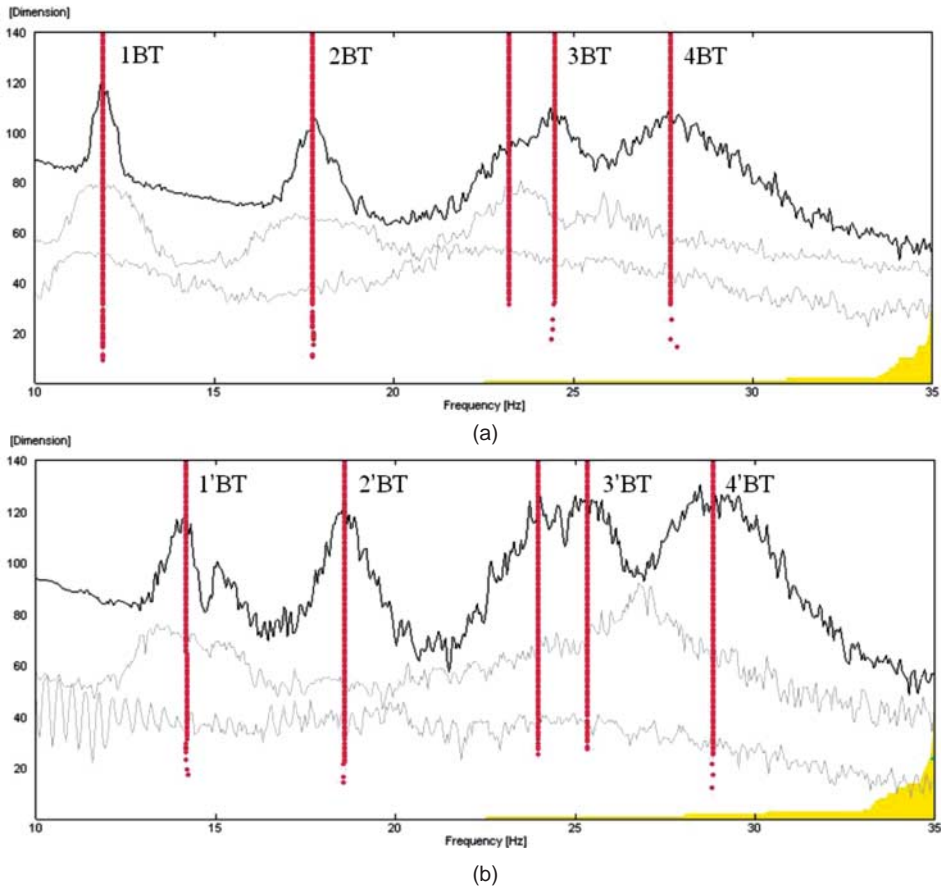
Figure 20. Identification of modal parameters through the SSI-DATA method: (a) bogie without dampers; (b) bogie with dampers.

(Figure 20(b)) of the primary suspension installed. The same figure indicates the alignments concerning four vibration modes identified in the test without dampers (modes 1BT to 4BT) and with dampers (modes 1′BT to 4′BT).

The inclusion of dampers resulted in the increase of frequency of all identified modes, with particular focus on the first mode (1BT and 1′BT) whose frequency has increased from 11.90 to 14.02 Hz, i.e. an increase of about 18%.

Figure 21 presents the values of the natural frequencies and the configurations of the identified modes. Modes 1BT/1′BT and 3BT/3′BT are longitudinal and transverse rotation modes, respectively. Mode 4BT/4′BT is a longitudinal rotation mode. Mode 2BT/2′BT is a translation mode whose motor axle's ordinates are higher than the trailer axle's ordinates. This is due to the non-uniform distribution of mass due to the reduction gear unit connected to the motor axle and partially supported by the crossbar.

4.3. *Passenger-seat system test*

The dynamic characteristics of the passenger-seat system were estimated based on a dynamic test involving the instrumentation with accelerometers placed on the seat cushion and on the seat structure next to their connection to the carbody (Figure 22(a)).

Mode 1BT (f_{1BT} = 11.90 Hz)   Mode 1'BT ($f_{1'BT}$ = 14.02 Hz)

Mode 2BT (f_{2BT} = 17.75 Hz)   Mode 2'BT ($f_{2'BT}$ = 18.60 Hz)

Mode 3BT (f_{3BT} = 24.48 Hz)   Mode 3'BT ($f_{3'BT}$ = 25.32 Hz)

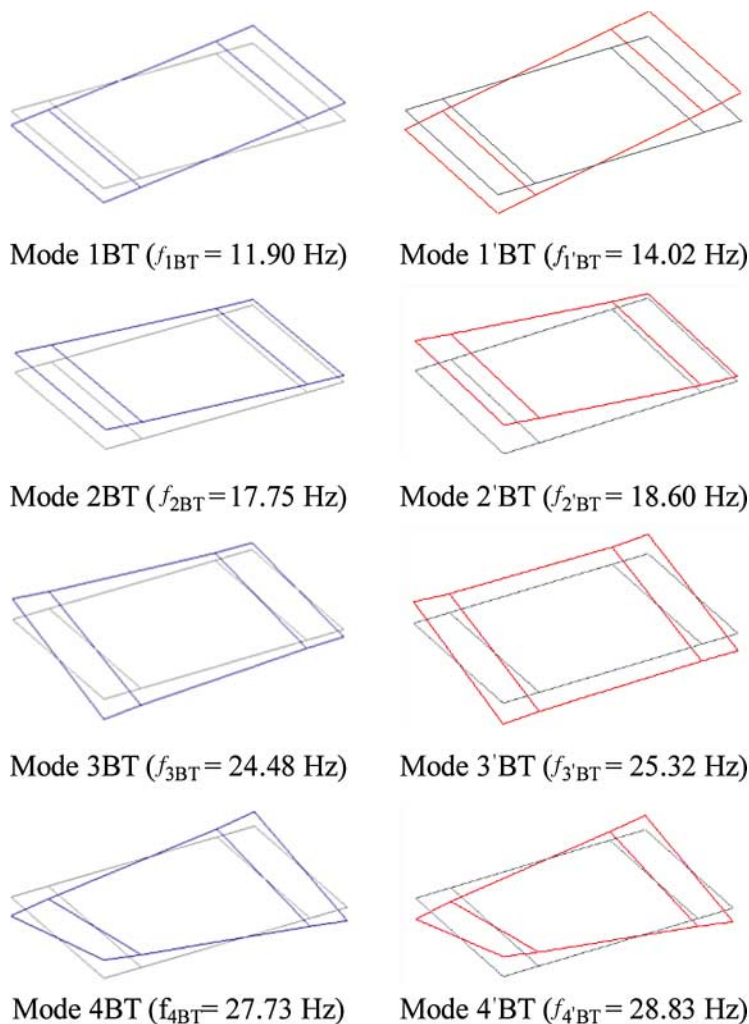Mode 4BT (f_{4BT} = 27.73 Hz)   Mode 4'BT ($f_{4'BT}$ = 28.83 Hz)

Figure 21.   Experimental frequencies and vibration modes of the bogie.

The PCB accelerometer, model 356B41, installed in the seat cushion has a circular flat shape, specially designed for placement in the passenger-seat interface. The test was performed with a passenger whose mass equals 80 kg. The excitation of the system was assured by a group of people who, in a random manner in time and space, jumped near the seat.

Figure 22(b) shows the experimentally and numerically determined transmissibility functions based on a one-DOF dynamic model whose calibration was based on the test results. This type of simplified models has been used by several authors such as Carlbom [22] and Wei and Griffin [28,29].

The best adjustment between the experimental and numerical curves was obtained for a stiffness of the seat equal to 58.4×10^3 N/m and a damping equal to 1658.6 Ns/m. The obtained values are within the same order of magnitude as the values estimated by Wei and Griffin [29] on experimental measurements performed on railway vehicles' seats. The curves show the existence of a function peak for a frequency equal to 4.28 Hz.
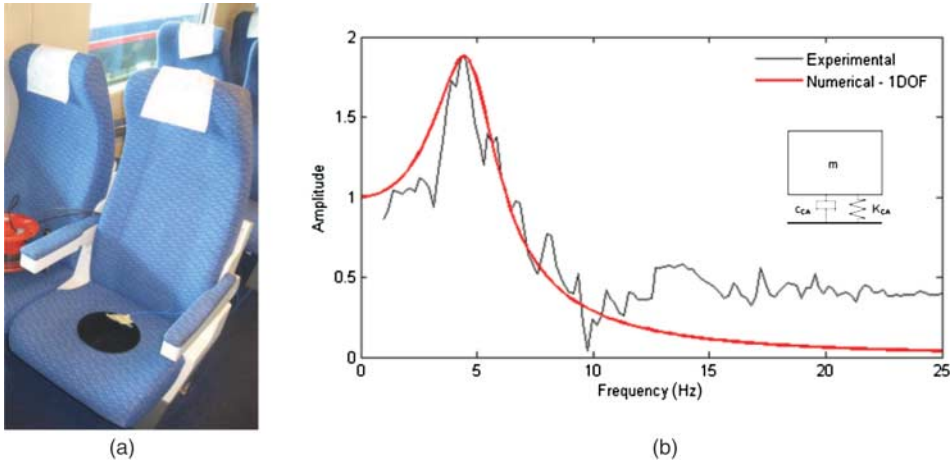
Figure 22. Dynamic test of the passenger-seat system: (a) PCB's triaxial accelerometer, model 356B4; (b) transmissibility function experimentally and numerically obtained based on a 1-DOF model.

5. Calibration methodology

5.1. *Computational implementation*

The calibration of the numerical model of the BBN vehicle was performed using an iterative method based on an optimisation technique [44]. This method consists on the resolution of an optimisation problem, which consists of the minimisation of an objective function by varying a set of the preselected model parameters. The preselection of the numerical parameters is carried out based on a global sensitivity analysis [33].

Figure 23 presents a flowchart illustrating the iterative method of calibration based on a genetic algorithm involving the use of three softwares: ANSYS [39], MATLAB [45] and OptiSlang [46]. The main aspects of the implemented calibration methodology are described in reference [47].

The calculation of modal parameters in systems with proportional damping matrix is based on a classic modal analysis [48,49]. In systems with non-proportional damping matrix the same calculation is based on a state-space formulation [50,51].

The mode-pairing technique aims to establish a correspondence between experimental and numerical vibration modes. This task is often complex due to alterations in the order of the numerical modes, resulting from variations on the numerical parameters which occur during the optimisation process and also due to the limited number of degrees of freedom of experimental modes, which increases the number of possible correspondence between numerical and experimental modes [36]. In this paper the correspondence between numerical and experimental modes is performed through an energetic criterion based on the modal strain energy and on the EMAC parameter [36,52]. The technique used for pairing complex vibration modes, based on the fundamentals of a state-space formulation, is addressed in Section 5.2.

The objective function (f) is defined based on the differences between the numerical and experimental modal parameters:

$$f = a \sum_{i=1}^{n} \frac{|f_i^{\text{exp}} - f_i^{\text{num}}|}{f_i^{\text{exp}}} + b \sum_{i=1}^{n} |\text{MAC}(\varphi_i^{\text{exp}}, \varphi_i^{\text{num}}) - 1|, \tag{3}$$

where f_i^{exp} and f_i^{num} are the experimental and numerical frequencies referring to mode i, ϕ_i^{exp} and ϕ_i^{num} are the vectors containing the experimental and numerical modal information related
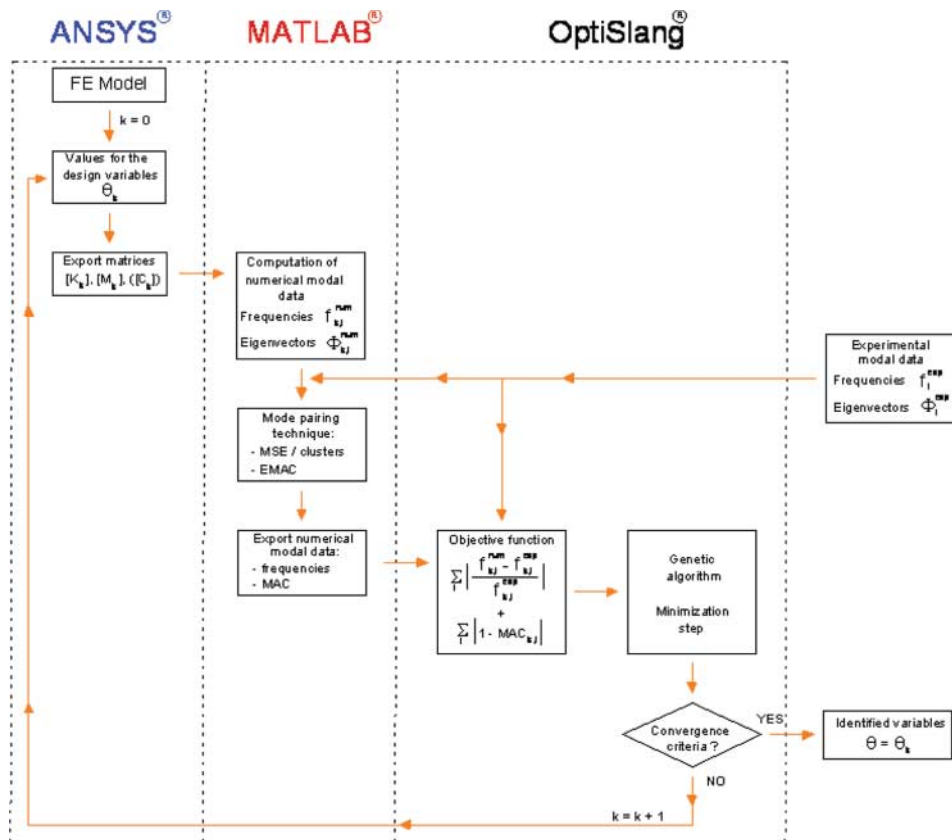
Figure 23.   Calibration methodology for the numerical model.

to mode i, a and b are weighting factors of the objective function terms and n is the total number of vibration modes.

5.2.   *Pairing technique of complex vibration modes*

The criterion based on the modal strain energy and on the EMAC parameter has been successfully applied in the pairing of systems with real vibration modes [36]. However, its application to systems with complex vibration modes, like railway vehicles, cannot be done directly, given that there are no orthogonality conditions of the vibration modes in relation to the mass and stiffness matrices [36].

The main theoretical foundations for the pairing technique of complex modes, proposed in this work, based on the application of a state-space formulation [51] are presented below.

In a state-space formulation the result from the orthogonality conditions are:

$$\Psi^{\mathrm{T}} \mathbf{Q} \Psi = \begin{bmatrix} \diagdown & b_j & \diagdown \end{bmatrix}, \tag{4}$$

where Ψ is the matrix containing the eigenvectors of the system which are related to the frequencies and vibration modes as follows:

$$\Psi = \begin{bmatrix} \Phi_1 & \cdots & \Phi_{n'} & \Phi_1^* & \cdots & \Phi_{n'}^* \\ \Phi_1 \lambda_1 & \cdots & \Phi_{n'} \lambda_{n'} & \Phi_1^* \lambda_1^* & \cdots & \Phi_{n'}^* \lambda_{n'}^* \end{bmatrix}, \tag{5}$$

where Φ and Φ^* are the vectors of the vibration modes in correspondence to frequencies λ_k and λ_k^*, which are conjugated pairs of complex numbers, n' is the number of vibration modes, **Q** is a matrix which incorporates the stiffness and mass matrices:

$$\mathbf{Q} = \begin{bmatrix} \mathbf{K} & 0 \\ 0 & -\mathbf{M} \end{bmatrix} \quad (6)$$

and b_j is a complex number.

Similar to the formulation proposed by Brehm *et al.* [36] this new formulation is also based on the calculation of the strain energy of clusters, i.e. degrees of freedom groups of the numerical model.

Based on the **Q** matrix it is possible to set up the Q_{kl} submatrices which connect the degrees of freedom of clusters k and l, as follows:

$$Q_{kl} = \begin{bmatrix} K_{kl} & 0 \\ 0 & -M_{kl} \end{bmatrix}. \quad (7)$$

The modal energy of the j vibration mode in relation to cluster k (MSE_{jk}) is calculated using the following expression:

$$\text{MSE}_{jk} = \frac{1}{2} \sum_{l=1}^{n} \Psi_{jk}^{\mathrm{T}} Q_{kl} \Psi_{jl}, \quad (8)$$

where Ψ_{jk} is the matrix containing the modal information of numerical modes j, corresponding to the degrees of freedom of cluster k; Ψ_{jl} is the matrix containing the modal information of numerical modes j, corresponding to the degrees of freedom of cluster l, and n is the total number of clusters.

The relative energy ($\prod_{jk}$) represents the parcel of total energy mobilised in vibration mode j considering only the degrees of freedom of cluster k. This parameter is a scalar whose value varies between 0 and 1 and is given by:

$$\prod_{jk} = \frac{|\text{MSE}_{jk}|}{|\text{MSE}_j|} = \frac{|\sum_{l=1}^{n} \Psi_{jk}^{\mathrm{T}} Q_{kl} \Psi_{ji}|}{|\Psi_j^{\mathrm{T}} Q \Psi_j|} \quad \text{with } \text{MSE}_j \neq 0. \quad (9)$$

The EMAC_{ijk} parameter results from the ponderation of the MAC_{ij} parameter [37] through the relative modal energy ($\prod_{jk}$) of the various clusters:

$$\text{EMAC}_{ijk} = \prod_{jk} \text{MAC}_{ij}. \quad (10)$$

A given experimental mode is paired with the numerical mode to which the highest value of the EMAC parameter corresponds.

6. Calibration

The experimental calibration of the numerical model of the BBN vehicle was performed based on modal parameters which were identified by the dynamic tests of the bogie and carbody. The first phase focused on the calibration of the numerical model of the bogie under test conditions. The second phase focused on the calibration of the complete numerical model of the vehicle. The numerical parameters of the bogie estimated in the first phase were assumed as deterministic parameters in the second phase.

6.1. *Calibration of the bogie*

6.1.1. *Numerical model under test conditions*

The calibration of the numerical model of the bogie forced the development of a model that would reproduce the specific conditions of the test (Figure 24). Changes to the original model involved the removal of springs and dampers from the secondary suspensions and from the tilting and load bolsters. Elements were also added to simulate the interface between the bogie and the actuation system, including distribution blocks and elastic blocks of the secondary suspensions. Rigid supports were introduced, at the contact point of the hydraulic actuators, with the ability to assume different positions, thus meeting the deviations of the contact point in the longitudinal (x) and transverse (z) directions. In the longitudinal direction the element which simulates the distribution block was divided into 10 sections, each with a length of 0.04 m, creating 11 possible positions for the support (positions 0–10). Positions 0 and 10 correspond to the support position located in the point with lowest and highest coordinate according to axis x, respectively. Rigid beam elements, each with a length of 0.05 m, were inserted in the direction which is transversal to the distribution block, to allow positioning of the support in two new positions (positions -1 and 1) corresponding to the lower and higher coordinates according to axis z, respectively.

The elastic blocks of the suspension were modelled by spring elements positioned in the vertical direction. The stiffness of the contact between distribution blocks and elastic blocks of the suspension was also modelled, in the x and z directions, through spring elements.

Table 6 describes the mechanical and geometrical parameters of the numerical model including designation, statistical distribution, adopted value and its corresponding unit. These parameters should be considered together with the parameters indicated in Table 4.

The value of the vertical stiffness of the secondary suspension's elastic block was estimated based on the elements of the project [53]. The position of the contact point with the actuation system, in longitudinal and transverse directions, may assume different values for the left and right hydraulic actuators. The longitudinal position of the actuator was limited to positions 2–8.
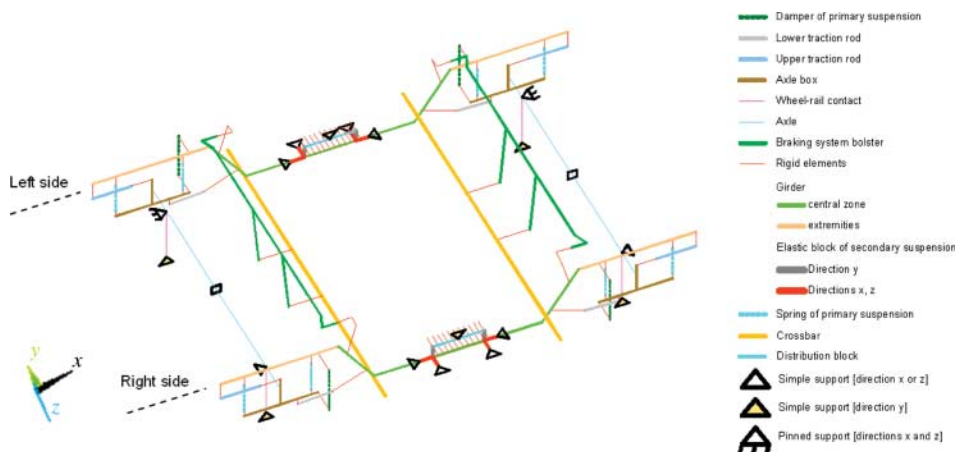

Figure 24.   Numerical model of the bogie under test conditions.

Table 6. Characterisation of the parameters of the numerical model of the bogie under test conditions.

Parameter	Designation		Type	Average value/ standard deviation	Limits (lower/upper)	Adopted value	Unit
				Statistical distribution			
K_b	Stiffness of the secondary suspension's elastic block	Dir y[a]	Uniform	12,000/1732	9000/15,000	12,000	kN/m
K_{btl}		Dir x and Dir z[a]	Uniform	25,250/14,289	500/50,000	5000	kN/m
Pos_{le}	Position of the contact point of the actuation system	Dir x[a] Left side	Uniform	5/1.7	2/8	5	–
Pos_{ld}		Right side					
Pos_{te}		Dir z[a] Left side	Uniform	0/0.6	−1/1	0	–
Pos_{td}		Right side					
E_m	Modulus of deformability of wood		Uniform	8/2.3	4/12	10	GPa

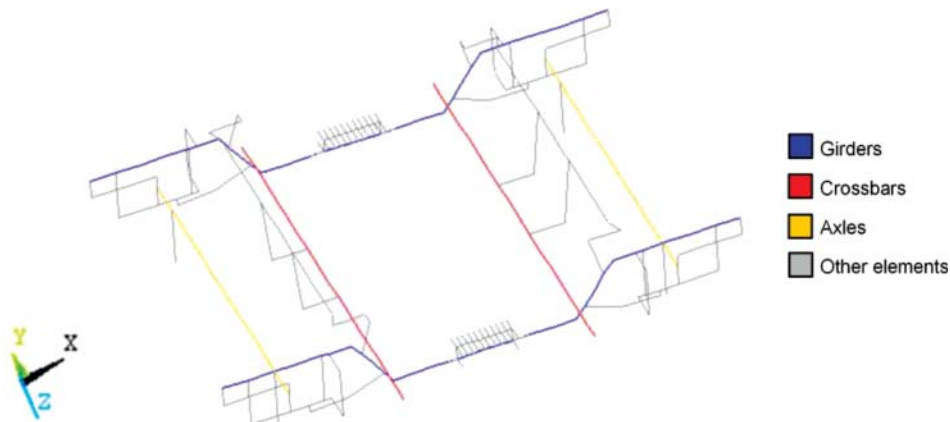[a]According to the referential of Figure 24.

Figure 25. Identification of clusters from the numerical model of the bogie under test conditions.

6.1.2. *Mode pairing*

Figure 25 presents the four clusters in which the model was divided for the mode pairing. The girders, crossbars and axles clusters only contain the degrees of freedom associated with the vertical direction (y). The remaining translation and rotation degrees of freedom were included in the other elements cluster.

Figure 26 shows the relative Modal Strain Energy (MSE) values for the various clusters and 30 numerical vibration modes, regarding the modal problem without damping (Figure 26(a)) and with damping (Figure 26(b)) of the suspensions.
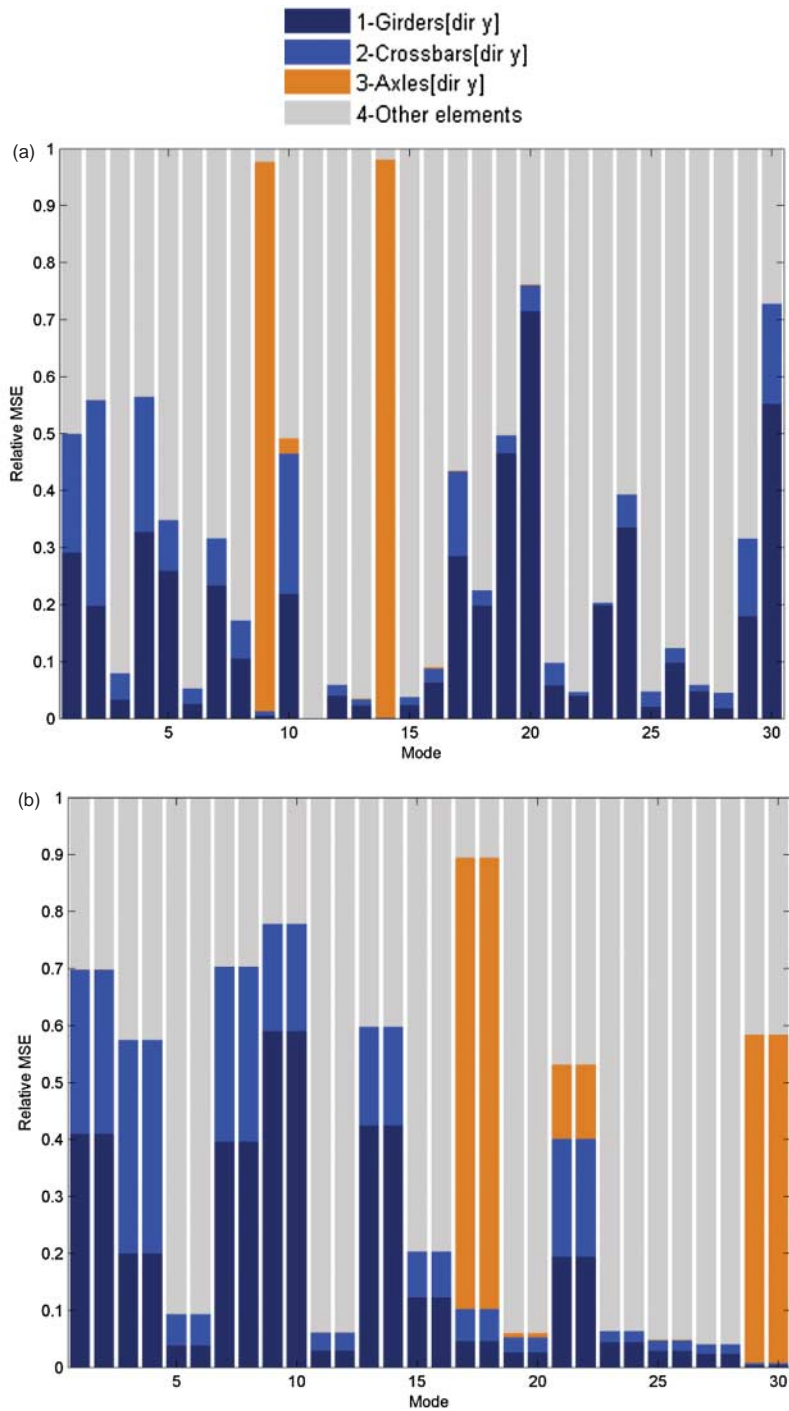
Figure 26. Values of relative MSE for the numerical vibration modes of the bogie under test conditions: (a) without damping; (b) with damping of the suspensions.

Figure 27 illustrates the MAC and EMAC correlation matrices of vibration modes, experimentally and numerically obtained, for cases without damping (Figure 27(a)) and with damping (Figure 27(b)) of suspensions.
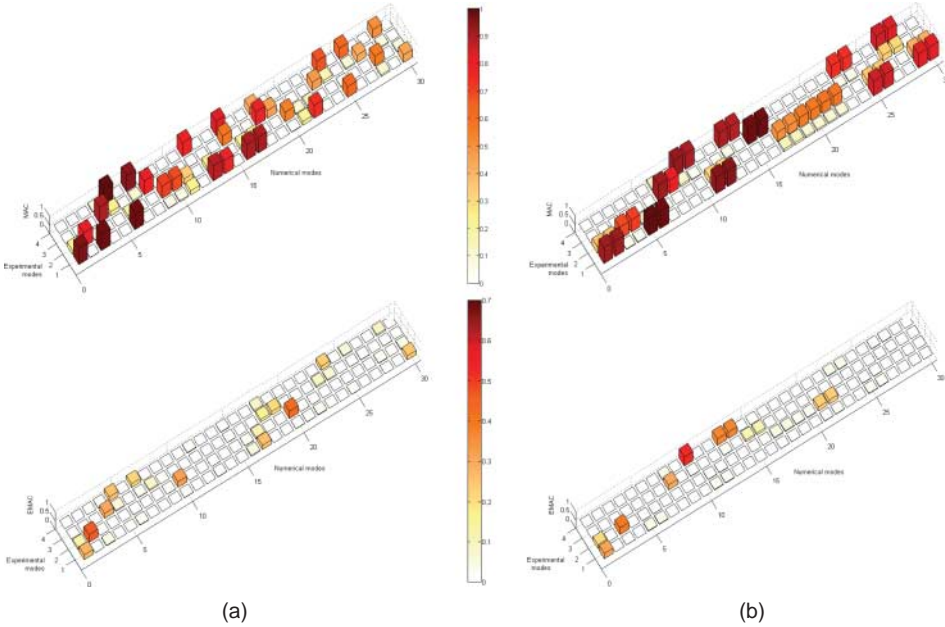
Figure 27. Correlation between the results of the initial numerical model of the tested bogie and the experimental results in terms of MAC and EMAC parameters for modal analysis: (a) without damping; (b) with damping of suspensions.

EMAC values of the various vibration modes, other than modes 2BT and 2′BT, were obtained by weighting MAC values for the modal strain energy of the cluster girders in direction y. This is the cluster that best relates to the positions and directions of the sensors used in the dynamic testing of the bogie. EMAC values of vibration modes 2BT and 2′BT resulted from weighting MAC values for the modal strain energy of clusters girders and crossbars in direction y.

The EMAC parameter facilitated the pairing of, virtually, all vibration modes, having been essential to the pairing of experimental modes 1BT, 1′BT and 4′BT. If, for example, the MAC parameter was used, experimental mode 1BT would be paired with numerical mode 3, which involves vibration of the support bolster of the braking system which, by structural compatibility, generates small amplitude rotational movements of the bogie. Based on the EMAC parameter, the correct match between experimental mode 1BT and numerical mode 1 was established. This is a global rotation mode that essentially mobilises the strain energy of the girders.

6.1.3. *Sensitivity analysis*

Figure 28 shows the results of the global sensitivity analysis using Spearman's rank correlation coefficient. This sensitivity analysis was performed using a stochastic sampling technique based on 500 samples generated by the Latin Hypercube method. This analysis was based on the parameters intervals presented in Tables 4 and 6. The correlation coefficients between $[-0.25, 0.25]$ were excluded from the graphical representation. The random generation of samples, particularly the parameters of the bogie's additional mass, was subject to the following restrictions:

$$-\varepsilon \leq \Delta M - [L_{lc}\Delta M_{lc} + L_{le}\Delta M_{le} + L_t\Delta M_t] \leq \varepsilon, \tag{11}$$

where ΔM equals 842 kg, and L_{lc}, L_{le} and L_t represent the total length of the central area of the girders, the extremities of the girders and crossbars, equal to 4.46 m, 3.56 m and 5.26 m, respectively, and ε is a tolerance considered equal to 150 kg.
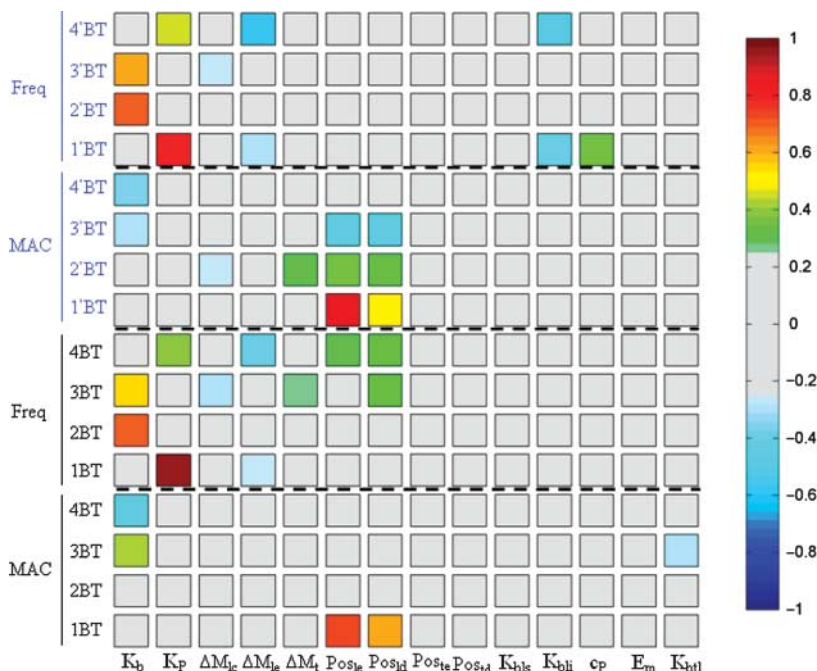
Figure 28. Spearman's rank correlation coefficient between the parameters and responses of the numerical model of the bogie under test conditions.

The correlation matrix shows that the stiffness of the primary suspensions, the additional mass of the girders (central area and extremities) and the stiffness of the lower traction rod of the axle box have significant influence over the vibration frequencies. In turn, the position of the actuators affects MAC values, particularly in modes 1BT/1′BT. The vertical stiffness of the secondary suspension blocks influences the vibration frequencies and also the MAC values in a significant way. The remaining analysed parameters do not have significant influence on the modal responses and were therefore excluded from the optimisation phase.

The influence of the primary suspensions' stiffness over the frequencies of modes 1BT/1′BT and 4BT/4′BT, for which the distance between the suspensions and the rotation axle of the bogie is larger, should be emphasised. In these modes the elastic block of the suspension has no influence over the responses due to its location near the rotation axle. It is not the case of the frequencies of modes 2BT/2′BT and 3BT/3′BT, which involve transverse translation and rotation of the bogie, respectively, and for which the stiffness of the suspension blocks, compared with the primary suspensions, is decisive for controlling the responses.

6.1.4. *Optimisation*

The optimisation of the model involved 10 numerical parameters (K_b, K_p, ΔM_{lc}, ΔM_{le}, ΔM_t Pos_{le}, Pos_{ld}, K_{bli}, c_p and K_{btl}) and 16 modal results (8 vibration frequencies and 8 MAC values). The genetic algorithm was based on an initial population of 30 individuals considering 250 generations, in a total of 7500 individuals. The initial population was randomly generated by the Latin Hypercube method. A number of elites equal to 1 and a number of substitute individuals also equal to 1 have been defined in this algorithm. The crossover rate was assumed to be 50% and the mutation rate was considered equal to 15% with a standard deviation variable along the optimisation between 0.10 and 0.01.
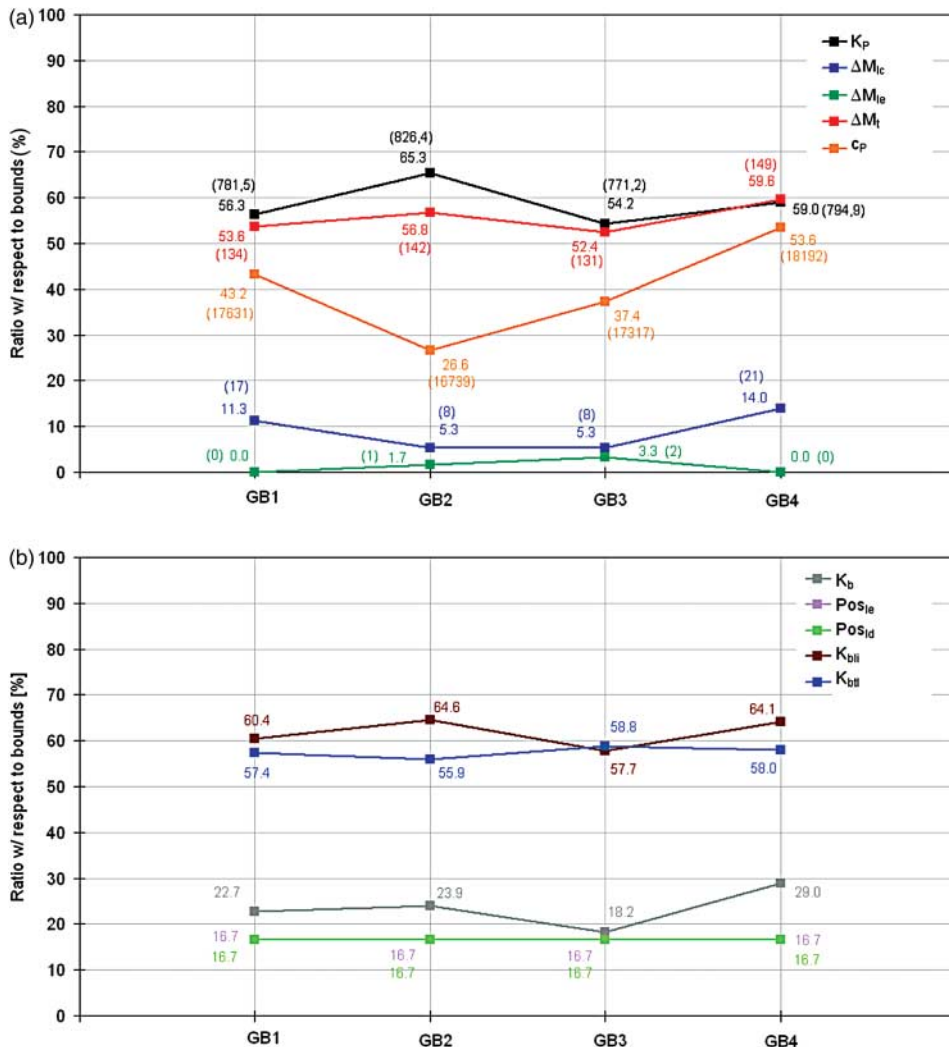
Figure 29. Values of numerical parameters for optimisation cases GB1–GB4: (a) stiffness and damping of the primary suspension and increment of masses; (b) characteristics of the elastic elements and actuation system.

The objective function is identical to that of Expression (3) considering a total number of vibration modes equal to 8 and weighting factors *a* and *b* equal to 1.

The optimisation problem still includes restrictions related to the parameters of additional mass of the bogie.

Optimal values of the parameters were obtained from the results of four independent optimisation cases (GB1–GB4) based on different initial populations. Figure 29 shows the ratios of the values of each parameter of the model in relation to the limits indicated in Tables 2, 4 and 6. The limits of the distributions of some of the parameters were extended, such as the cases of the stiffness of the primary suspension (500/1000 kN/m), and the stiffness of the axle box's traction rods (3/10 and 10/40 MN/m) due to the systematic tendency of the optimum solutions of these parameters to reach the limits indicated in Table 4. A 0% ratio means that the parameter coincides with the lower limit. A ratio of 100% means that it coincides with the upper limit. The stiffness and damping parameters of the primary suspension and increments of mass are presented in Figure 29(a) indicating, in brackets, the numerical parameters' values.
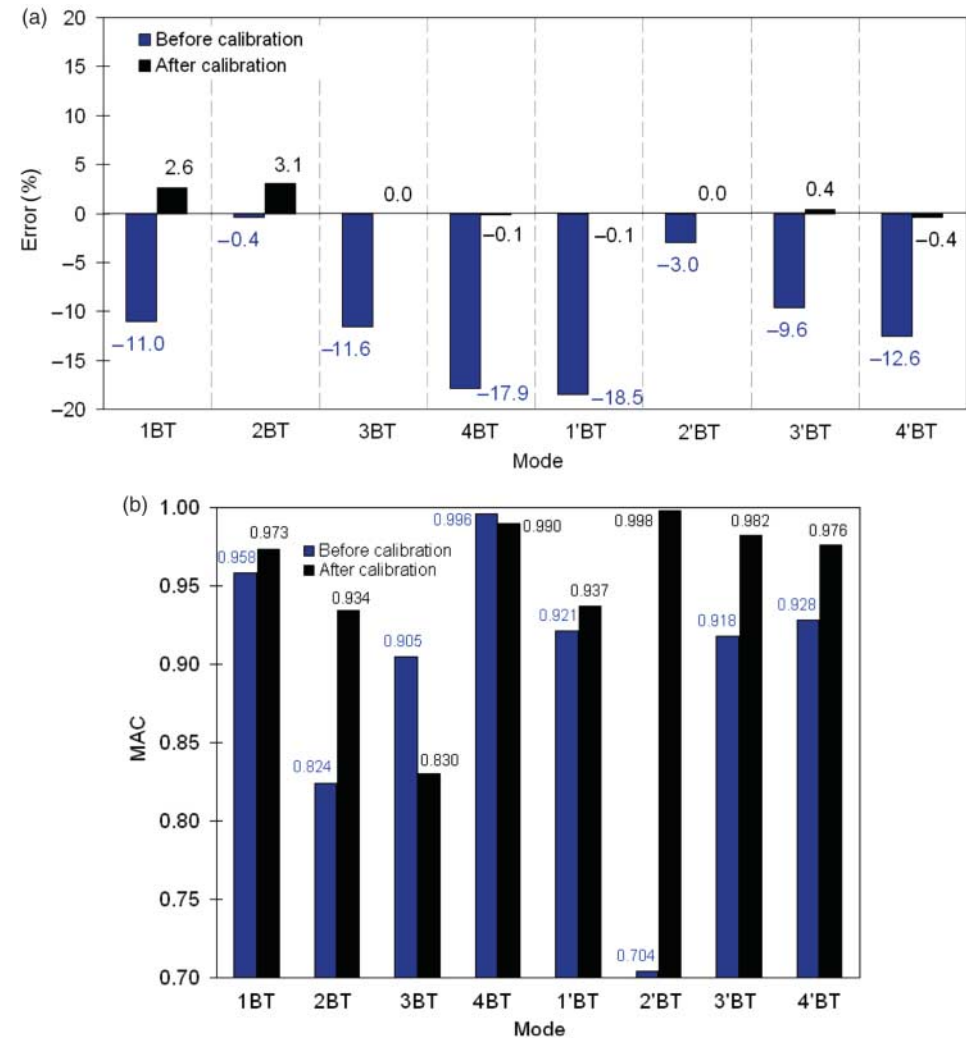
Figure 30. Comparative analysis of the errors of experimental and numerical responses, before and after calibration: (a) vibration frequencies; (b) MAC.

The parameters related to the elastic elements (blocks and rod) and actuation system are shown in Figure 29(b).

The analysed parameters present a good stability with variations below 10%, except for the damping of the primary damper. This is one of the parameters that the sensitivity analysis has shown to have a smaller influence over the numerical responses.

Figure 30 summarises the error values between the numerical and experimental vibration frequencies, taking as reference the average values of the experimental frequencies, and the values of the MAC parameter, before and after calibration.

The results after calibration are related to optimisation case GB2, which was the one presenting the lowest residual of the objective function. The average error of the frequencies decreased from 10.6% before calibration to 0.8% after calibration. In turn, the average value of the MAC parameter increased from 0.894 before calibration to 0.953 after calibration.

As visualised in Figure 31, the experimentally obtained and numerically derived optimised modal configurations of the bogie coincide almost perfectly.
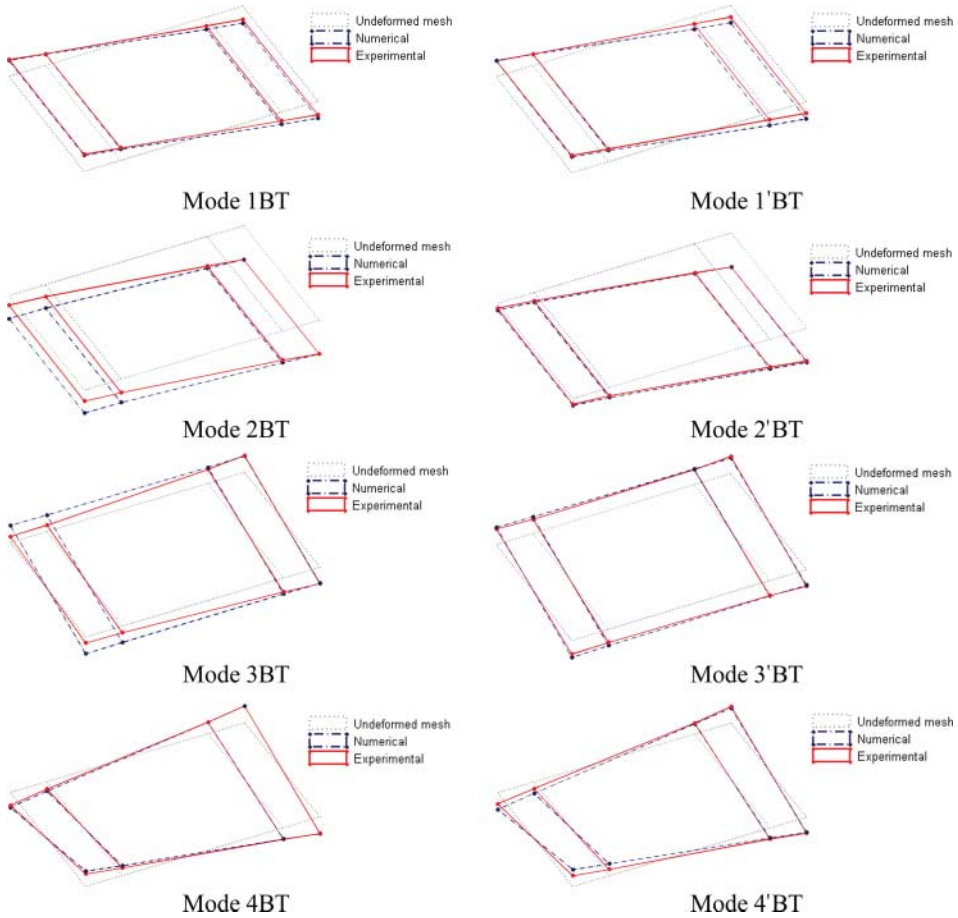
Figure 31.   Comparison between the experimental and numerical vibration modes of the bogie after calibration.

6.2.   *Calibration of the complete model of the BBN vehicle*

6.2.1.   *Sensitivity analysis*

Figure 32 presents the results of the global sensitivity analysis using Spearman's rank correlation coefficient. The sensitivity analysis was performed using a stochastic sampling technique based on 250 samples generated by the Latin Hypercube method. This analysis was based on the parameters intervals presented in Table 2. The random generation of samples, particularly for the parameters of the carbody's additional mass, was subject to the following restrictions:

$$-\varepsilon \le 100 - [\Delta M_b + \Delta M_p + \Delta M_c] \le \varepsilon, \tag{12}$$

where ΔM_b, ΔM_p and ΔM_c represent the additional mass on the base, side walls and cover, respectively, and ε is a tolerance equal to 10%. The mode pairing was performed by application of a technique based on the modal strain energy and on the EMAC parameter.

The correlation matrix shows that the stiffness of secondary suspensions, from front (K_{S1}) and rear (K_{S2}) bogies, has significant influence over the frequencies and MAC values of the rigid body modes of the carbody. In turn, the RMI parameters from the base (RMI$_b$) and side walls (RMI$_p$) essentially control the frequencies and MAC values of the structural modes of the carbody. The parameters additional mass (ΔM_b, ΔM_c and ΔM_p) and stiffness of the
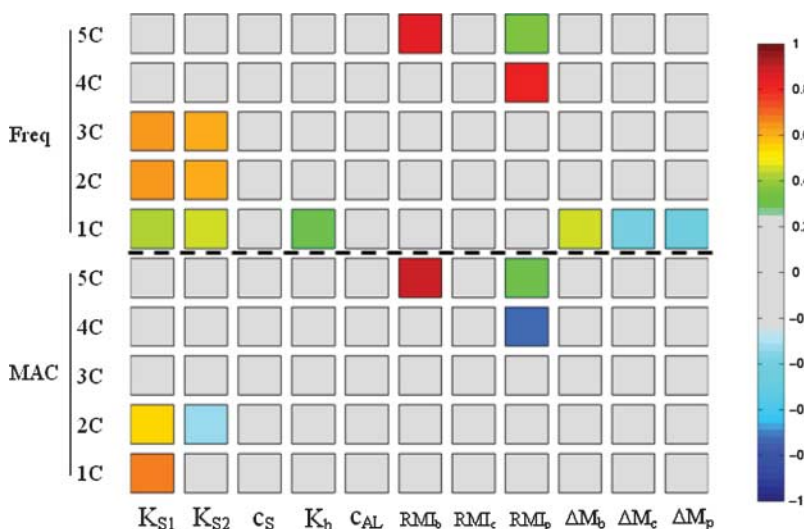
Figure 32. Spearman's rank correlation coefficient between the parameters and responses of the carbody's numerical model.

connecting rod between the tilting and load bolsters (K_b) have significant influence over the vibration frequency of mode 1C. The remaining analysed parameters did not have significant influence with respect to the modal responses, and were consequently excluded from the optimisation phase.

It is possible to verify that the flexural stiffness of the side walls, which is controlled by the walls' RMI parameter, is important for controlling the torsional stiffness of the carbody, as demonstrated by the high value of the correlation coefficient between the walls' RMI parameter and the frequency of mode 4C.

6.2.2. *Optimisation*

The optimisation of the model involved 7 numerical parameters (K_{S1}, K_{S2}, RMI_b, RMI_p ΔM_b, ΔM_c and ΔM_p) and 10 modal results (5 vibration frequencies and 5 MAC values). The control parameters of the genetic algorithm and the objective function are identical to those in the optimisation of the bogie. The only difference is related to the total number of modes considered in the objective function, in this case equal to 5. The optimisation problem also included constraints involving the carbody's additional mass parameters. The mode pairing was performed by the application of a technique based on the modal strain energy and on the EMAC parameter.

Optimal values of the parameters were obtained from the results of four independent optimisation cases (GC1–GC4) based on different initial populations. Figure 33 shows the values' ratios of each parameter of the model in relation to the limits given in Table 2. The lower and upper stiffness limits of the secondary suspension were extended from 242 and 272.9 kN/m to 200 and 400 kN/m, respectively. Parameters related to the characteristics of the secondary suspension, connecting rod and geometrical properties of the carbody are presented in Figure 33(a) indicating, in brackets, the estimated values for the stiffness of the secondary suspension. The parameters referring to mass distribution are presented in Figure 33(b).

It is noticeable that the most stable parameters, with variations below 10%, are those that most affect the responses, including the stiffness of secondary suspensions and RMI parameters
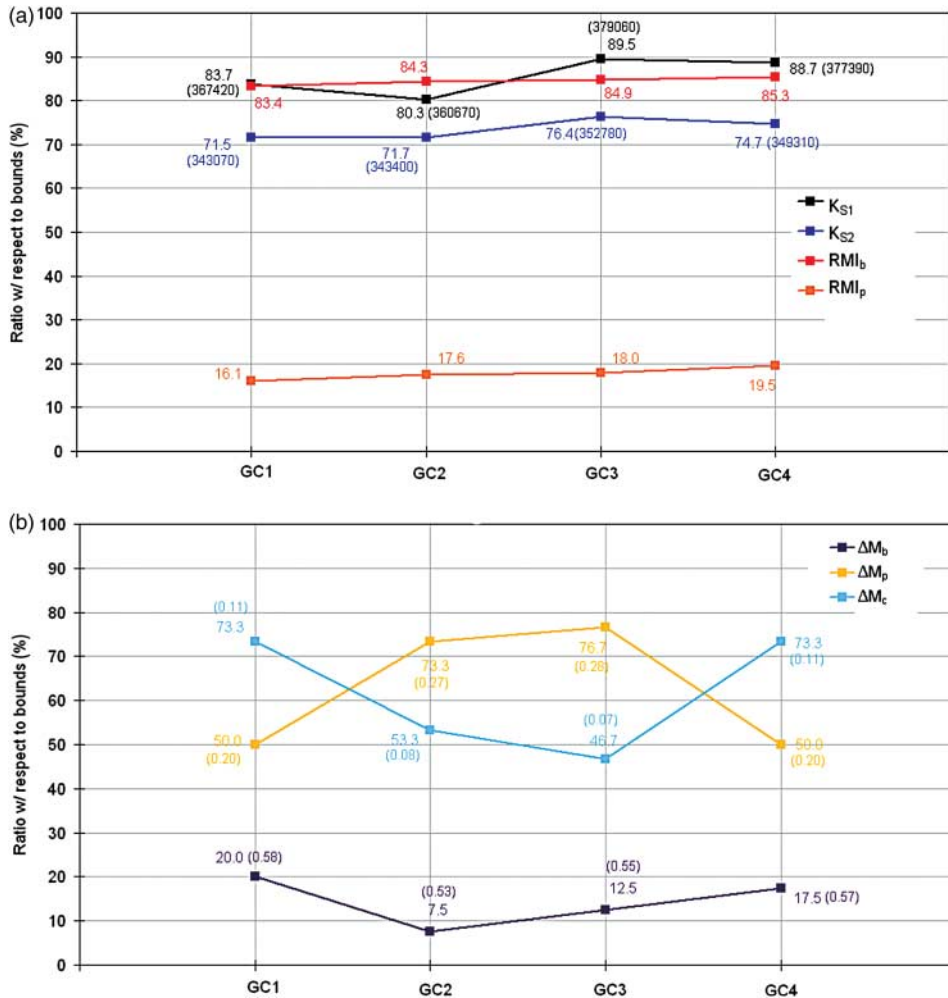
Figure 33. Values of numerical parameters for optimisation cases GC1–GC4: (a) characteristics of the suspension, connecting rods and geometrical properties of the carbody; (b) masses.

of the base and side walls. The stiffness values of the front bogie's secondary suspension are higher than those estimated for the rear bogie.

Regarding the additional masses of the side walls and cover, the estimates show higher variations, close to 25%. This should be related to the fact that these parameters contribute in a similar way to the participant mass on vibration mode 1C. Therefore, there may be different combinations of these parameters leading to the same solution, in terms of optimisation of the problem.

Figure 34 summarises the error values of the numerical and experimental vibration frequencies taking as reference the average values of the experimental frequencies, and of the MAC parameter, before and after calibration. The results after calibration are related to the GC1 optimisation case, which was the one with the lowest final residual of the objective function. The frequencies' average error dropped from 20.3%, before calibration, to 2.9%, after calibration. This error decrease is mainly due to the reduction of the error associated with the frequencies of structural modes 4C and 5C. The average value of the MAC parameter did not change significantly, increasing from 0.927, before calibration, to 0.937, after calibration.

The excellent agreement between the carbody's experimentally obtained and numerically derived optimised modal configurations can be verified in Figure 35.

6.3. *Final results*

The combination between the numerical parameters, obtained for the optimisation case of the bogie GB2, and the parameters obtained in optimisation case of the complete vehicle GC1, were the basis for the establishment of the vehicle's calibrated numerical model.

Table 7 presents the values of the damped vibration frequencies of the main vibration modes of the BBN vehicle obtained from the calibrated numerical model.

Comparing the values of the frequencies with the values given in Table 5, concerning the initial numerical model, there is a visible tendency towards the frequency increase on the rigid body modes of the carbody and bogies, being that, in the bogies' case, this increase ranged from 10% to 55%. This tendency is due to the significant increase of the stiffness of the primary
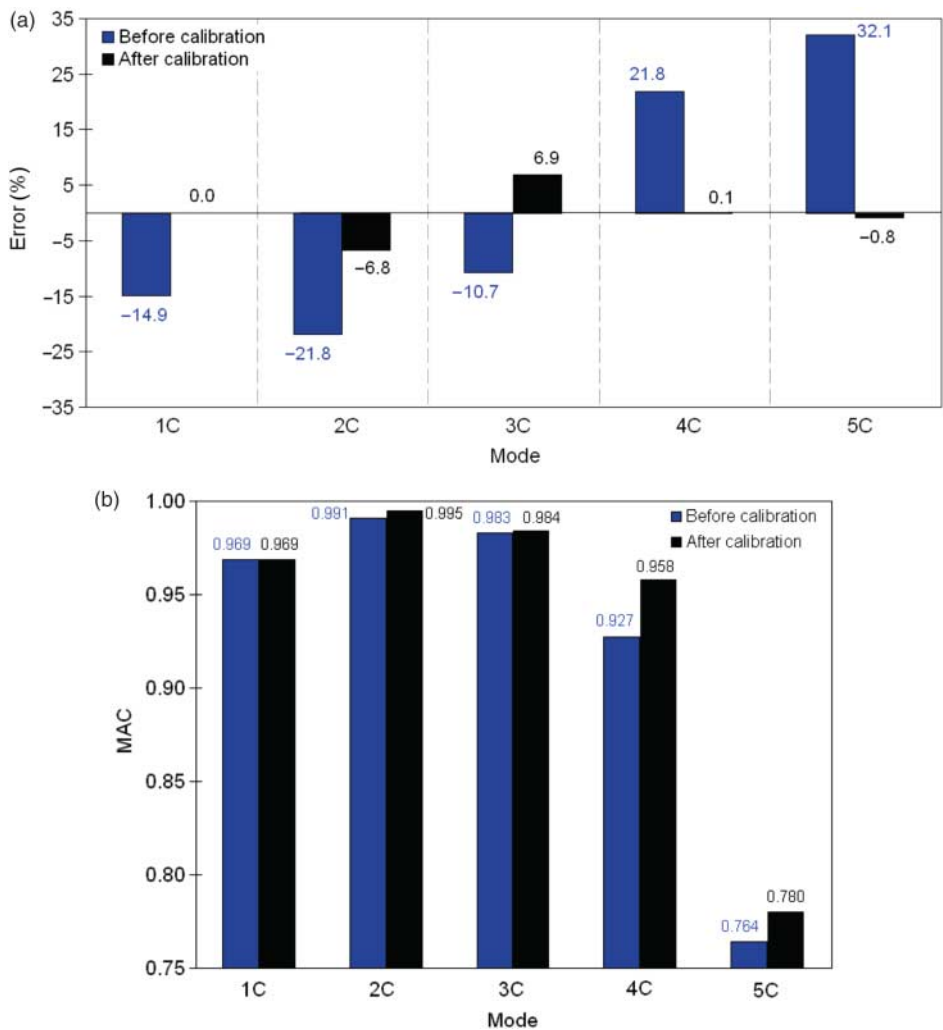

Figure 34. Comparative analysis of the errors from the experimental and numerical responses, before and after calibration in terms of: (a) vibration frequencies; (b) MAC.
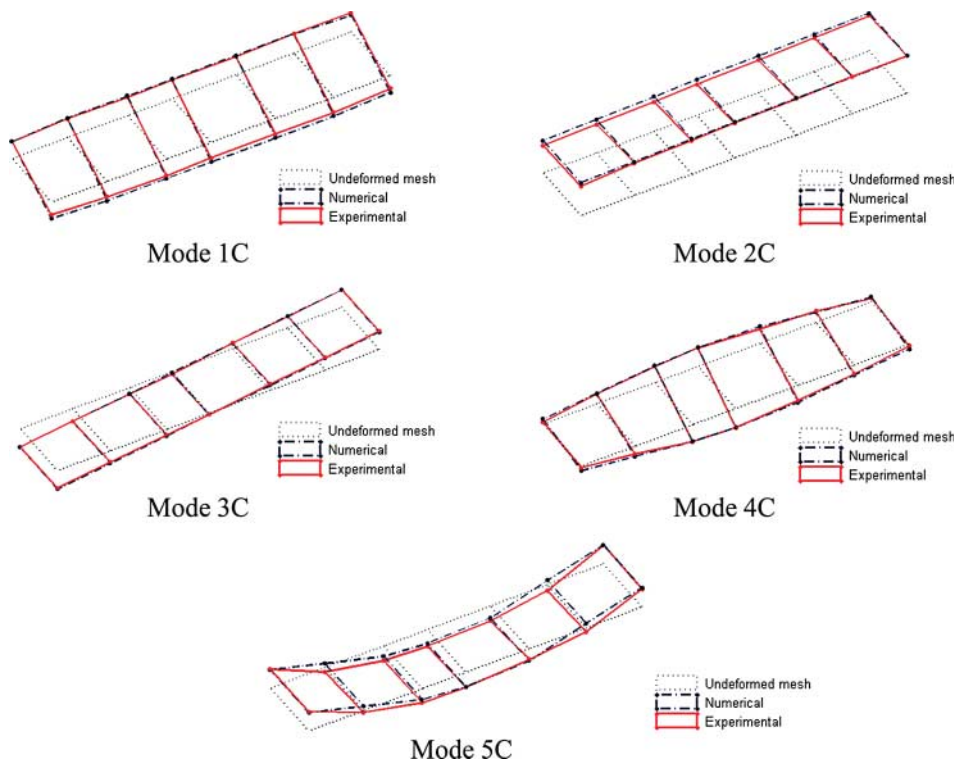
Figure 35. Comparison between the vibration modes of the carbody, experimentally and numerically obtained, after calibration.

Table 7. Natural frequencies of the BBN vehicle obtained from the calibrated numerical model.

Element	Mode	Damped frequency (Hz)
Carbody	1C	1.01
	2C	1.24
	3C	1.70
	4C	8.39
	5C	12.16
	6C	17.73
Bogies	1B	9.21/9.24
	2B	7.70/8.12
	3B	14.16/14.09

and secondary suspension springs. In turn, the structural modes of the carbody, particularly modes 4C and 5C showed a decreased tendency of approximately 20%, mainly due to the reduction of the RMI parameter of the carbody's side walls.

7. Conclusions

This paper described the experimental calibration of the numerical model of a BBN vehicle of the Alfa Pendular train based on modal parameters. The dynamic tests performed on the vehicle and bogie allowed the identification of frequencies and modal configurations of a

large number of vibration modes involving rigid body and structural movements. The bogie test results showed that the inclusion of primary dampers led to an increase of the frequencies of the identified vibration modes, particularly of the longitudinal rotation mode. The dynamic test of the seat also permitted to identify the vibration frequency of the passenger-seat system, close to 4.3 Hz, and estimate the stiffness and damping parameters.

The calibration of the numerical model was conducted through an iterative methodology based on an optimisation algorithm and was performed using a submodelling/multistep approach involving two phases: the first phase focused on the calibration of the model of the bogie under test conditions and the second focused on the calibration of the complete model of the vehicle.

Global sensitivity analysis allowed the identification of numerical parameters to be considered in the calibration. The parameters that have showed the highest sensitivities in relation to the modal responses were, for the bogie, the vertical stiffness of the secondary suspension block and the vertical stiffness of the primary suspensions. As for the carbody, the RMI parameters of the base and side walls and the vertical stiffness of the secondary suspension were the parameters with highest sensitivity in relation to the modal responses.

The optimisation of the numerical model was conducted using a genetic algorithm involving a total of 17 numerical parameters and 26 modal responses (13 vibration frequencies and 13 MAC values). The results of the optimisation cases of the bogie and vehicle, based on different initial populations, led mostly to very stable numerical parameters' values, particularly for those highly correlated with the responses.

The comparison between the numerical vibration frequencies' values, before and after calibration, and the experimental vibration frequencies, has revealed significant improvements on the initial numerical models. The average error of vibration frequencies of the modes of the bogie under test conditions went from 10.6%, before calibration, to 0.8%, after calibration. Concerning the vibration modes of the complete model of the vehicle, the average error of frequencies went from 20.3%, before calibration, to 2.9% after calibration. Significant improvements were also observed in MAC values, particularly in the vibration modes of the bogie. This result demonstrates the robustness and efficiency of genetic algorithms on the estimation of the vehicle's modal responses.

The combination of numerical parameters obtained for the GB2 bogie optimisation case with the parameters obtained for the GC1 case of vehicle optimisation provided the basis for developing the calibrated numerical model of BBN vehicle. Compared with the initial numerical model, the calibrated numerical models show higher frequency values of the rigid-body modes of the carbody and bogies, essentially due to the increased stiffness of the primary and secondary suspension springs. On the other hand, most of the carbody's structural modes tended to decrease, largely due to a reduction of the RMI parameter of the side walls of the vehicle's carbody.

In future studies, the calibrated numerical model of the vehicle will be used to access the dynamic behaviour of the train-track coupled system, in terms of passengers comfort and wheel–rail contact stability, on plain track, on bridges or on transition zones.

Acknowledgements

References

[1] L. Auersch, *The excitation of ground vibration by rail traffic: Theory of vehicle–track–soil interaction and measurements on high-speed lines*, J. Sound Vib. 284 (2005), pp. 103–132.

[2] M. Baeßler, J. Bronsert, P. Cuéllar, and W. Rücker, *The stability of ballasted tracks supported on vibrating bridge decks, abutments and transition zones*, First international conference on railway technology: Research, development and maintenance, Las Palmas, Spain, 2012.

[3] ERRI D214/RP9, *Railway bridges for speeds >200 km/h*, Final Report, European Rail Research Institute (ERRI), Utrecht, Netherlands, 2001.

[4] L. Frýba, *Dynamics of Railway Bridges*, Thomas Telford, Prague, 1996.

[5] H. Xia and N. Zhang, *Dynamic analysis of railway bridge under high-speed trains*, Comput. Struct. 83 (2005), pp. 1891–901.

[6] T. Dahlberg, *Railway track stiffness variations – consequences and countermeasures*, Int. J. Civil Eng. 8 (2010), pp. 1–12.

[7] D. Li and D. Davis, *Transition of railroad bridge approaches*, J. Geotech. Geoenviron. Eng. 131 (2005), pp. 1392–1398.

[8] J. Kwark, E. Choi, Y. Kim, B. Kim, and S. Kim, *Dynamic behavior of two-span continuous concrete bridges under moving high-speed train*, Comput. Struct. 82 (2004), pp. 463–474.

[9] T. Tomioka and T. Takigami, *Reduction of bending vibration in railway vehicle carbodies using carbody–bogie dynamic interaction*, Veh. Syst. Dyn. 48 (2010), pp. 467–486.

[10] J. Pombo, *A multibody methodology for railway dynamics applications*, Doctoral thesis, IST, Lisbon, Portugal, 2004.

[11] D. Hanson, *Operational modal analysis and model updating with a cyclostationary input*, Doctoral thesis, University of New South Wales, 2006.

[12] A. Stribersky, F. Moser, and W. Rulka, *Structural dynamics and ride comfort of a rail vehicle system*, Adv. Eng. Softw. 33 (2008), pp. 541–552.

[13] Q. Li, Y. Xu, D. Wu, and Z. Chen, *Computer-aided nonlinear vehicle-bridge interaction analysis*, J. Vib. Control 16 (2010), pp. 1791–1816.

[14] L. Yu, H. Zhu, and J. Yang, *A modelling approach for the lightweight design of railroad truck*, 12th IFToMM World Congress, Besançon, France, 2007.

[15] P. Carlbom, *Combining MBS with FEM for rail vehicle dynamics analysis*, Multibody Syst. Dyn. 6 (2001), pp. 291–300.

[16] Y.-S. Wu, Y.-B. Yang, and J.-D. Yau, *Three-dimensional analysis of train–rail–bridge interaction problems*, Veh. Syst. Dyn. 36 (2001), pp. 1–35.

[17] Y.-S. Lee and S.-H. Kim, *Structural analysis of 3D high-speed train–bridge interactions for simple train load models*, Veh. Syst. Dyn. 48 (2010), pp. 263–281.

[18] T. Tomioka, T. Takigami, and Y. Suzuki, *Numerical analysis of three-dimensional flexural vibration of railway vehicle car body*, Veh. Syst. Dyn. 44 (2006), pp. 272–285.

[19] S. Popprath, C. Benatzky, C. Bilik, M. Kozek, A. Stribersky, and J. Wassermann, *Experimental modal analysis of a scaled car body for metro vehicles*, 13th International Congress on Sound and Vibration, Vienna, Austria, 2006.

[20] T. Tomioka, Y. Suzuki, and T. Takigami, *Three-dimensional flexural vibration of lightweight railway vehicle carbody and a new analytical method for flexural vibration*, Quartely Report of RTRI, 2003; 44, Number 1.

[21] S. Iwnicki, *Handbook of Railway Vehicle Dynamics*, Taylor & Francis, London, 2006.

[22] P. Carlbom, *Carbody and passengers in rail vehicle dynamics*, Doctoral thesis, KTH – Royal Institute of Technology, Stockholm, Sweden, 2000.

[23] G. Diana, F. Cheli, A. Collina, R. Corradi, and S. Melzi, *The development of a numerical model for railway vehicles comfort assessment through comparison with experimental measurements*, Veh. Syst. Dyn. 38 (2002), pp. 165–183.

[24] J.-S. Kim and J.-C. Jeong, *Natural frequency evaluation of a composite train carbody with lenght of 23 m*, Comput. Sci. Technol. 66 (2006), pp. 2272–2283.

[25] M. Kozec, C. Benatzky, A. Schirrer, and A. Stribersky, *Vibration damping of a flexible car body structure using piezo-stack actuators*, 17th World Congress The International Federation of Automatic Control, Seoul, Korea, 2008.

[26] D. Wennberg, *A light weight car body for high-speed trains* (Literature study), KTH – Royal Institute of Technology, Stockholm, Sweden, 2009.

[27] O. Dossing, *Dynamic design verification of a prototype rapid transit train using modal analysis*, Technical report, Bruel&Kjaer, 1984.

[28] L. Wei and J. Griffin, *The prediction of seat transmissibility from measures of seat impedance*, J. Sound Vib. 214 (1998), pp. 121–137.

[29] L. Wei and J. Griffin, *Mathematical models for the apparent mass of the seated human body exposed to vertical vibration*, J. Sound Vib. 212 (1998), pp. 855–874.

[30] M. Mehrpouya and H. Ahmadian, *Estimation of applied forces on railway vehicle wheelsets from measured vehicle responses*, Int. J. Veh. Struct. Syst. 1 (2009), pp. 104–110.

[31] Y. He and J. Mc Phee, *Optimization of the lateral stability of rail vehicles*, Veh. Syst. Dyn. 38 (2002), pp. 361–390.
[32] H. Ahmadian, *Extracting modes of a railway vehicle from measured responses*, IOMAC, Orlando, 2005.
[33] A. Saltelli, S. Tarantola, F. Campolongo, and M. Rato, *Sensitivity Analysis in Practice: A Guide to Assessing Scientific Models*, John Wileys & Sons, Ltd, New York, 2004.
[34] V. Zabel and M. Brehm, *System identification of high-speed railway bridges*, Weimar Optimization and Stochastic Days, Weimar, Germany, 2009.
[35] X. Yu and M. Gen, *Introduction to Evolutionary Algorithms*, Springer, London, 2010.
[36] M. Brehm, V. Zabel, and C. Bucher, *An automatic mode pairing strategy using an enhanced modal assurance criterion based on modal strain energies*, J. Sound Vib. 329 (2010), pp. 5375–5392.
[37] R. Allemang, *The modal assurance criterion – twenty years of use and abuse*, J. Sound Vib. 37 (2003), pp. 14–21.
[38] Politecnico di Torino, *Studio di specifici problemi inerenti le attività produttive connesse al trasporto su rotala, con particolare approfondimento ai contenuti tecnologici dello stabilimento ALSTOM Savigliano*, Dipartimento di Meccanica, Torino, 2000.
[39] ANSYS, *Structural Analysis Guide – Release 11.0*, ANSYS, Inc, Torino, 2007.
[40] CP, *Desenhos de projecto e características técnicas do comboio Alfa Pendular*, Direcção de Material, Fiat Ferroviaria, Italy, 2001 (in portuguese).
[41] EN 1999-1-1, *Eurocode 9: Design of aluminium structures – Part 1-1: General structural rules*, CEN, Brussels, 2007.
[42] D. Nguyen, K. Kim, and P. Warnitchai, *Simulation procedure for vehicle-substructure dynamic interactions and wheel movements using linearized wheel–rail interfaces*, Finite Elem. Anal. Des. 45 (2009), pp. 341–356.
[43] ARTeMIS, *ARTeMIS Extractor Pro – Academic Licence*, User's Manual, Structural Vibration Solutions ApS, Aalborg, Denmark, 2009.
[44] M. Brehm, *Vibration-based model updating: Reduction and quantification of uncertainties*, Doctoral thesis, Bauhaus Universitat Weimar, Weimar, Germany, 2011.
[45] Mathworks, *MATLAB – Getting Started Guide*, Natick, 2011.
[46] OptiSLang, *OptiSLang – the Optimizing Structural Language*, 3.0 edition, Dynardo GmbH Weimar, Germany, 2008.
[47] D. Ribeiro, R. Calçada, R. Delgado, M. Brehm, and V. Zabel, *Finite element model updating of a bowstring-arch railway bridge based on experimental modal parameters*, Eng. Struct. 40 (2012), pp. 413–435.
[48] R. Clough and J. Penzien, *Dynamics of Structures*, 2nd ed., McGraw Hill, New York, 1993.
[49] D. Ewins, *Modal Testing: Theory and Practice*, 2nd ed., Research Studies Press, London, 2000.
[50] C. Hoen, *An engineering interpretation of the complex eigensolution of linear dynamic systems*, IMAC XXIII, Orlando, 2005.
[51] F. Magalhães, *Identificação modal estocástica para validação experimental de modelos numéricos*, Master thesis,. Porto, FEUP-UP, 2003 (in portuguese).
[52] M. Brehm, V. Zabel, C. Bucher, and D. Ribeiro, *An automatic mode selection strategy for model updating using the modal assurance criterion and modal strain energies*, 18th International Conference on the Application of Computer Science and Mathematics in Architecture and Civil Engineering, Weimar, Germany, 2009.
[53] CP, *Comboio Eléctrico Pendular Série 4000*, 1998 (in portuguese).